Monthly Notices
of the
ROYAL ASTRONOMICAL SOCIETY

Mon. Not. R. Astron. Soc. **408,** 580–600 (2010) doi:10.1111/j.1365-2966.2010.17146.x

The stable archipelago in the region of the Pallas and Hansa dynamical families

V. Carruba★

UNESP, Univ. Estadual Paulista, Grupo de Dinâmica Orbital e Planetologia, Guaratinguetá, SP 12516-410, Brazil

Accepted 2010 June 4. Received 2010 June 4; in original form 2010 April 6

ABSTRACT

Among highly inclined asteroids, the region of the central main belt between the 3J:–1A and 5J:–2A mean-motion resonances has long been known to host the Pallas and Hansa dynamical families. This region is characterized by the presence of the ν_6, ν_5 and ν_{16} secular resonances, which in conjunction with the 8J:–3A mean-motion resonance divide the area into eight regions, the stable islands of the archipelago. Using a set of proper elements available at the Asteroids Dynamic Site (AstDyS) at the time, Gil-Hutton identified a family around (686) Gersuind and two more minor clumps around (945) Barcelona and (148) Gallia in the space of synthetic proper elements. In this work I compute a new set of synthetic proper elements for 2310 numbered and 2142 multi-opposition objects in this region. The use of the frequency-modified Fourier transform method allowed me to obtain non-negative estimates of the proper frequency of argument of pericentre precession g for members of the Hansa families characterized by values of $e_{\rm forced}$ larger than $e_{\rm free}$, and to solve the problem of the non-linear dependence of g versus n observed by Carruba & Michtchenko.

My analysis shows that the two minor clumps of Gil-Hutton should now be considered dynamical families. Also, a new family in the domains of both proper elements (a, e, $\sin i$) and frequencies (n, g, $g + s$) around (1222) Tina is discovered in this work, as well as a new frequency family around (4203) Brucato. Nine minor clumps, one of which is visible in both domains, are also observed.

The taxonomical analysis of family members suggests that the Pallas family is compatible with a B-type composition (but two members are classified as C interlopers), while the Hansa family is possibly an S-type one. Sloan Digital Sky Survey Moving Object Catalog (SDSS-MOC3) data suggest that the Barcelona family might be an Sq group, and the Gersuind, Gallia and Tina ones should belong to the S complex. Geometric albedo data seem to confirm the possibility that the Barcelona and Gersuind families belong to the S complex. Data on cumulative size distributions, collisions time-scales, rotation rates and dynamics in this region are also revised in this work.

Key words: celestial mechanics – minor planets, asteroids: general.

1 INTRODUCTION

Among highly inclined asteroids (asteroids with $\sin i > 0.3$, for which the analytical theory used to obtain proper elements is not very accurate: Milani & Knežević 1994), the asteroids in the region of the Pallas and Hansa families are characterized by very interesting dynamics. This region is characterized by the presence of the ν_6, ν_5 and ν_{16} secular resonances, which in conjunction with the 8J:–3A mean-motion resonance divide the area into eight regions, the stable islands of the archipelago.

In these islands, the Pallas family was first suggested by Williams (1992) and Lemâitre & Morbidelli (1994), while the largest family in the region, Hansa, was originally proposed by Hergenrother, Larson & Spahr (1996). Gil-Hutton (2006) defines the region of the Pallas and Hansa families (zone B in his paper) as the region between the 3J:–1A and 5J:–2A mean-motion resonances (which roughly corresponds to the region between 2.501 and 2.825 au) and with $\sin i > 0.3$. As discussed in Knežević & Milani (2000), although it is not possible to obtain accurate analytical proper elements for this region, even some of the synthetic ones, as is the case for some low-eccentricity members of the Hansa family (Carruba & Michtchenko 2009), are affected by errors: objects with free eccentricity smaller than the forced one present difficulties in obtaining accurate values

★E-mail: vcarruba@feg.unesp.br

of the pericentre precession frequency g. The presence of linear resonances in the region, such as the ν_5, ν_6, ν_{16} and other non-linear resonances, also introduces difficulties in obtaining accurate values of proper elements and frequencies.

However, having an accurate data set of proper elements is essential to obtain dynamical families and clumps, and, in general, to investigate the local dynamics. In this paper I therefore first tried to obtain synthetic proper elements, not only for the numbered asteroids in the region, for which such elements are already listed within the Asteroids Dynamic Site (AstDyS)[1], but also for multi-opposition objects. Using the frequency-modified Fourier transform method of Šidlichovský & Nesvorný (1997) and the method described in Knežević & Milani (2000) for obtaining synthetic proper elements and frequencies, I also tried to obtain better estimates of proper g for those Hansa asteroids that appeared to have retrograde values in the AstDyS data set (Carruba & Michtchenko 2009). Overall, I obtained synthetic proper elements for 4452 asteroids in the region of the Hansa and Pallas families.

As a next step I identified families in the space of proper elements and proper frequencies using the Classical and Frequency Hierarchical Clustering Systems (CHCM and FHCM, respectively: Zappalà et al. 1995; Carruba & Michtchenko 2007, 2009). Family subgroups and asteroid-pair candidates (Pravec & Vokrouhlický 2009) were also detected in the region, and the data on taxonomy and Sloan Digital Sky Survey Moving Object Catalog (SDSS-MOC3) data for family members were reviewed. Analysis of the data on geometric albedo, absolute magnitude, cumulative distributions and collision time-scales, Yarkovsky isolines and C-target functions, light curves and dynamics in the region was also carried out, following the approach of Carruba (2009).

This work is set out as follows: the first section introduces the problems of dynamical families in the highly inclined central main belt. In the second section I discuss how the set of proper elements for asteroids in the region was obtained, and I compare my results with those available in the literature (namely at the AstDyS site). In the third section I obtain dynamical families and clumps in the domains of proper elements and proper frequencies, and candidates for possible broken asteroid pairs, while in the fourth section I discuss the taxonomy of asteroids in this area. In the fifth section I revise the current knowledge on asteroid albedos and absolute magnitudes, while the sixth section deals with cumulative distributions of family members. In the seventh section I obtain Yarkovsky isolines and C-target functions for the observed families. The eighth section analyses the data on rotation for the bodies for which such information is available, and the ninth section discusses the dynamics present in this region, with an emphasis on non-linear secular resonances and their effects. In the final section I present my conclusions.

2 SYNTHETIC PROPER ELEMENTS FOR ASTEROIDS IN THE PALLAS REGION

If we want to study the dynamical evolution of asteroid groups in the Pallas region, the first step is to determine their dynamical family in the space of proper elements (Bendjoya & Zappalà 2002) and proper frequencies (Carruba & Michtchenko 2007, 2009). For this purpose it is necessary to have a catalogue of asteroids for which proper elements were determined either analytically (Milani & Knežević 1994) or numerically (also called synthetic elements: Knežević & Milani 2003). For highly inclined asteroids ($\sin i > 0.3$) the analytical theory is not accurate enough to provide reliable proper elements, so one has to rely on the synthetic ones. The AstDyS site offers, as of 2009 November 25, a list of 214 414 asteroids for which proper elements and frequencies are available, as well as the standard deviation of the proper elements and frequencies.[2] Of these objects, 2336 have orbits in the region of the Pallas family as defined in Gil-Hutton (2006). Using the catalogue of proper elements available at the time, Gil-Hutton (2006) obtained families and clumps in the space of proper elements for asteroids in the region of the Pallas family, among others.

A problem with this approach is that several of the asteroids in the region reported by the AstDyS site have large errors in the proper frequencies, and many of them, especially in the Hansa family region, are characterized by negative values of the pericentre precession frequency g. This is caused, as discussed in Knežević & Milani (2003), by the fact that high-inclination and low-eccentricity objects may have their equinoctial elements ($e\cos\varpi$, $e\sin\varpi$) passing through zero, which makes a correct determination of the proper frequency g harder. This problem is of particular concern for asteroids with free eccentricity smaller than the forced one, since the motion of ϖ in (h, k) space, which describes a circle of radius $e_{\rm free}$ (which for synthetic proper elements coincides with $e_{\rm proper}$) centred at the point of a vector of magnitude $e_{\rm forced}$, may cover only a limited range of values rather than 2π, making it more difficult to obtain reliable values of the proper frequency g (Murray & Dermott 1999).

Fig. 1 displays plots of amplitude (in arbitrary units) versus frequency for the spectra of the Fourier transforms of equinoctial elements (h, k) of (a) (36) Atalante and (b) (480) Hansa. The first asteroid is characterized by a relatively large value of proper eccentricity (0.2747), but the second has a rather small proper eccentricity (0.0091). While the frequency spectra of the first asteroid are dominated by the proper frequency g, the values of planetary frequencies are larger than the asteroid proper one for the second body. This makes obtaining reliable values of synthetic proper frequencies g for such a class of bodies a difficult task, as discussed by Knežević & Milani (2000). More information on the values of proper frequencies in the region will be given in Section 2.1.

Also, strong secular resonances such as the $\nu_5 = g - g_5$, $\nu_6 = g - g_6$, $\nu_7 = g - g_7$ or resonance of arguments $2g - 2s$ for low-eccentricity objects may affect the current determination of proper values of g for asteroids in the region (but with relatively minor errors in the proper elements $(a, e, \sin i)$. Knežević & Milani (2003) distinguish between 'stable' proper elements with relatively small errors (see Section 2.1 for a definition of 'small errors'), unstable proper elements and pathological cases, characterized by extremely large uncertainties in proper elements. Understanding the stability of proper elements in the complicated region of the Pallas family is of great importance if one wants to obtain reliable dynamical families.

To investigate this problem in this work, I decided to obtain my own set of proper elements for numbered objects, following the

[1] http://hamilton.dm.unipi.it/astdys

[2] Proper elements and frequencies were obtained with a 10-Myr numerical integration with a Burlisch–Stoer integrator. The elements were then computed over a 2-Myr period, and a running-box method was used to produce 10 data points. The values of proper elements and frequencies were the means of the data points, while as an approximation of the error the standard deviation was used. See Knežević & Milani (2003) for further details on the subject.

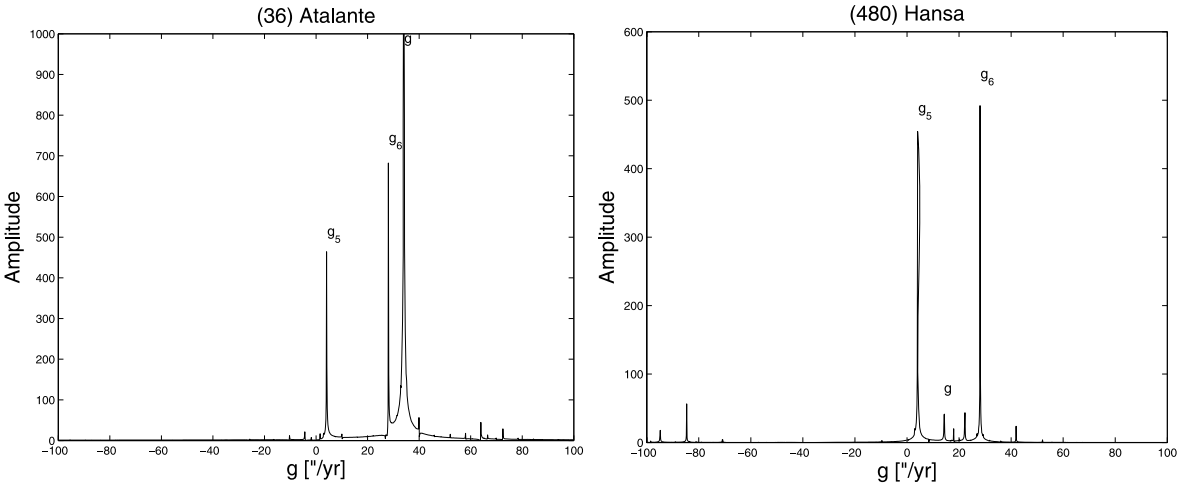

Figure 1. Amplitude (in arbitrary units) versus frequency for the spectra of the Fourier transform of equinoctial elements (h, k) of (a) (36) Atalante and (b) (480) Hansa.

approach of Knežević & Milani (2003) (proper frequencies were obtained using the frequency-modified Fourier transform (FMFT) of Šidlichovský & Nesvorný (1997) on the osculating equinoctial elements of the integrated asteroids), and to compare my results with those obtained by the two authors. I first downloaded the catalogue of osculating elements for numbered and multi-opposition asteroids and the catalogue of synthetic proper elements and frequencies from the AstDyS site,[3] accessed on 2009 November 25. At that time there were 140 235 asteroids in the catalogue of multi-opposition objects.

I integrated the 2336 numbered objects in the Pallas region and 4320 objects in the multi-opposition catalogue (asteroids with semi-major axis between the 3J:–1A and 5J:–2A mean-motion resonances and with an osculating inclination larger than 15°) with a Burlisch–Stoer integrator from the SWIFT package (Levison & Duncan 1994) modified by Brož (1999) so as to include on-line digital filtering to remove all frequencies with period less than 600 yr, and I integrated the objects over 10 Myr. Synthetic proper elements were obtained with the procedure described in Knežević & Milani (2003), except for the proper frequencies, which were derived with the FMFT using the following procedure: I eliminated from the spectra of the Fourier transform of the equinoctial elements all planetary frequencies and then assigned as proper frequency the largest value in the spectra that was still observable, rather than fitting the time series of $\varpi_{\rm f}$ and $\Omega_{\rm f}$ of the oscillations in the (k, h) and (p, q) plane.

As regards numbered objects, I first eliminated from my data set the 21 asteroids that did not survive the length of the integration. Five more objects that interacted with powerful mean-motion resonances and that had large errors (see next subsection) in proper elements as a result were also excluded from the data set. In order to calibrate the procedure for finding synthetic proper elements, we first need to compare the results of the numerical simulation for numbered objects with the proper elements in the AstDyS site. For this purpose, we need to revise the properties of the AstDyS proper elements in the region, which I will do in the next subsection.

2.1 Synthetic proper elements in the AstDyS catalogue

I start by analysing the behaviour of proper elements in the AstDyS catalogue. As discussed in Milani & Knežević (1994), asteroids with large standard deviation in the proper semi-major axis σ_a are usually associated with two- or three-body mean-motion resonances. The large standard deviation in a is caused by the averaging needed to produce the proper elements for asteroids involved in libration inside a resonance.

Fig. 2 displays (a) (a, e) and (b) (a, $\sin i$) projections of the AstDyS proper elements for the 2310 objects in the area (the 2336 objects minus the 21 that did not survive the 10-Myr integration and the five objects with large errors in their proper elements). Small full dots display asteroids with σ_a between 0.0003 au (the limit given by Knežević & Milani (2003) for 'stable' synthetic proper elements) and 0.01 au (the limit for pathological cases), while large full dots show asteroids with σ_a larger than 0.01 au. The magenta line displays the chaotic layer near 3J:–1A studied by Guillens, Vieira Martins & Gomes (2002), as defined in Morbidelli & Vokrouhlický (2003). Vertical red lines display the location of some of the most important two- and three-body mean-motion resonances in the region, while blue lines show the location of the main linear secular resonances, computed using the frek.f code of Milani & Knežević (1994) to compute the proper frequencies g and s for the grid of (a, e) and (a, $\sin i$) values shown in Fig. 2 and the values of angles and eccentricity for (480) Hansa. Non-linear secular resonances will be discussed in detail in Section 9 and later on in this section. The inclined blue and red lines shown in the (a, e) plane display the area where the pericentre of the asteroid is equal to the apocentre and pericentre of Mars, respectively.

As can be seen in the figure, one can easily identify the groups in the (a, $\sin i$) plane associated with the Hansa and Pallas families. Families in the (a, $\sin i$) plane appear to be confined in inclination because, as discussed in Michtchenko et al. (2010), to change the plane of its orbits an asteroid must gain several orders of kinetic energy more than the quantity necessary to produce a similar change in proper semi-major axis or eccentricity. Additionally, the Yarkovsky effect predominantly acts on the asteroid semi-major axis. Asteroids with large σ_a are associated with prominent mean-motion resonances such as the 8J:–3A, 1J:–3S–1A and 1J:2S:–2A. Object at high eccentricities with σ_a larger than 0.001 are likely to be associated with asteroids on planet-crossing orbits.

Due to the presence of the strong linear secular resonances ν_6, ν_5 and ν_{16}, in conjunction with the effect of the powerful 8J:–3A mean-motion resonance, eight regions, the stable islands of the archipelago, can be distinguished, each one identified by the lowest

[3] http://hamilton.dm.unipi.it/cgi-bin/astdys/astibo

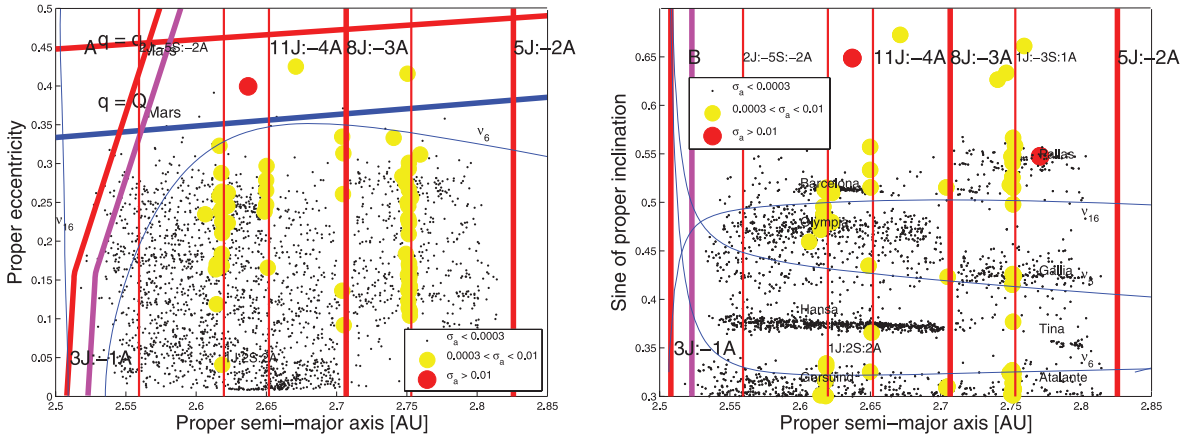

Figure 2. (a) An (a, e) projection of AstDyS asteroids in the region of the Pallas family. Small full dots display asteroids with standard deviation in σ_a between 0.0003 and 0.01, while large full dots show asteroids with σ_a larger than 0.01. (b) An $(a, \sin i)$ projection of the same asteroids.

numbered object in the area. From top to bottom in inclination they are the Barcelona region (above the ν_{16} secular resonance in inclination and between the 3J:–1A and 8J:–3A mean-motion resonances in semi-major axis), the Pallas region (above the ν_{16} resonance in inclination and on the right side of the 8J:–3A mean-motion resonance in semi-major axis), the Olympia region (between the ν_{16} and ν_5 resonances and on the left side of 8J:–3A), the Gallia region (in the same interval of inclination values as the Olympia region, but on the right side of the 8J:–3A resonance), the Hansa region (between the ν_5 and ν_6 resonances in inclination, and on the left side of the 8J:–3A mean-motion resonance in semi-major axis), the Tina region (the same as the Hansa region in inclination, but on the right side of the 8J:–3A mean-motion resonance in a) and the Gersuind and Atalante regions, below the ν_6 resonances and on the right and left sides of the 8J:–3A mean-motion resonance in a, respectively. All regions are marked in Fig. 2(b) and will be discussed in more detail in Section 3.

In Fig. 3 I display $(e, \sin i)$ projections of asteroids with values of the errors in (a) e and (b) i for 'stable' (black dots), 'unstable' (small full dots) and 'pathological' (large full dots) proper elements. As in Fig. 2, blue lines display the location of the main secular resonances in the region. As can be seen in the figure, errors in eccentricity and inclination are larger for asteroids at high inclination, with a few objects with large errors at low eccentricities that will be discussed in Section 2.2.

More important are the errors in proper frequencies. Fig. 4 displays (a) (a, g) and (b) (a, s) projections of AstDyS asteroids in the region of the Pallas family. Small full dots display asteroids with standard deviations of σ_g and σ_s between 1 and 10, while large full dots show asteroids with σ_g and σ_s larger than 10. Here I decided to plot g and s as functions of a rather than n to allow a more easy comparison of these figures with Fig. 2. As can be seen in the figure, while errors in s are uniformly spread among the observed asteroids, the errors in g are large and confined to negative or small values of g. For the Hansa family, as discussed in Carruba & Michtchenko (2009), negative values of g are related to objects with small eccentricities ($e < 0.0179$) and to the problem of determining correct proper elements for asteroids with equinoctial elements (k, h) passing through zero. The reliability of the negative g values from the AstDyS site for this region will be discussed in more detail in the next subsection.

Finally, I checked the total number of asteroids with completely 'stable' proper elements, i.e. with proper elements with small (as defined in this section) errors in a, e, $\sin i$, n, g and s, and found a total

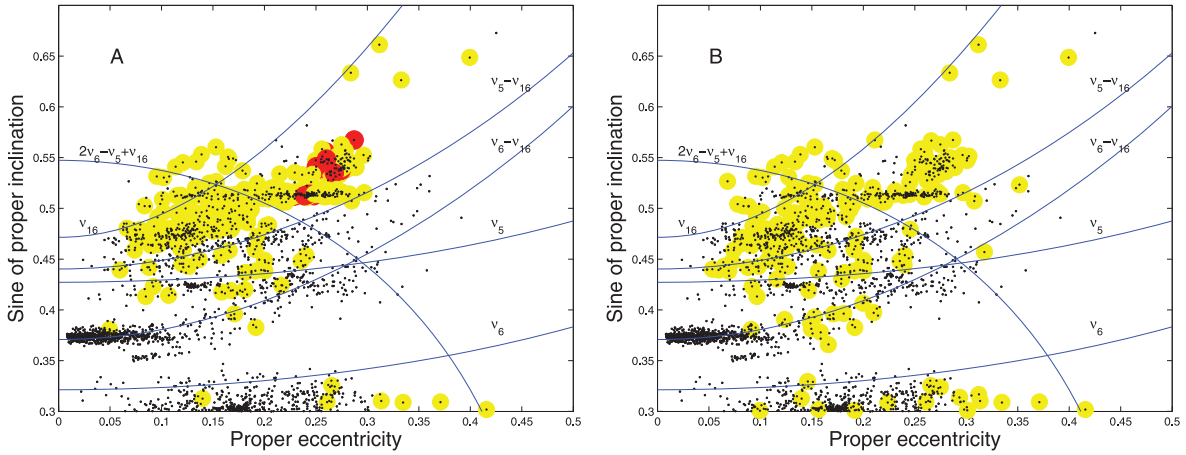

Figure 3. (a) An $(e, \sin i)$ projection of AstDyS asteroids in the region of the Pallas family. Small full dots display asteroids with standard deviation in σ_e between 0.003 and 0.1, while large full dots show asteroids with σ_e larger than 0.1. (b) An $(e, \sin i)$ projection of the same asteroids, but this time small full dots display asteroids with standard deviation in σ_i between 0.001 and 0.03, while large full dots show asteroids with σ_i larger than 0.03.

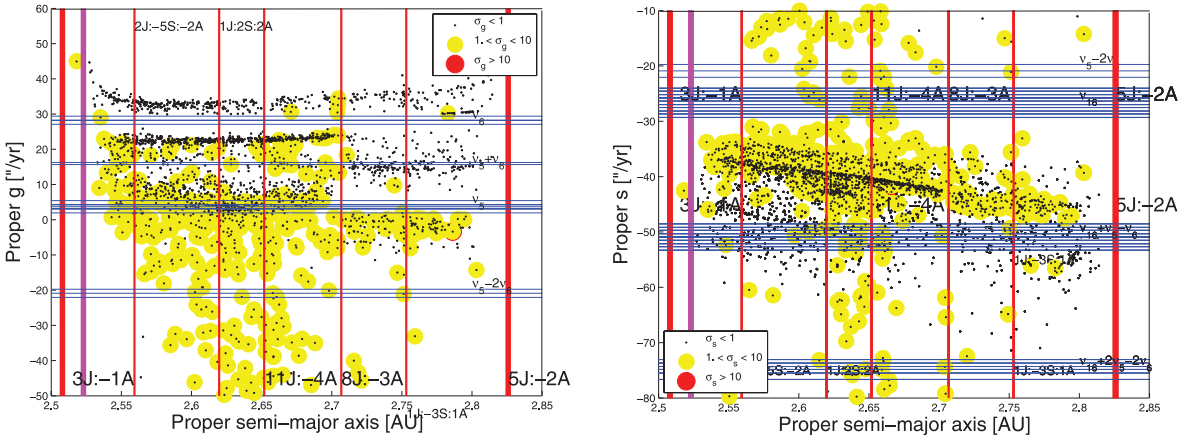

Figure 4. (a) An (a, g) projection of AstDyS asteroids in the region of the Pallas family. Small full dots display asteroids with standard deviation in σ_g between 1 and 10, while large full dots show asteroids with σ_g larger than 10. (b) An (a, s) projection of the same asteroids.

of 1475 objects. Further analysis of this number will be performed in the next subsection.

2.2 Numerically obtained synthetic proper elements

Once I had obtained my own set of proper elements for the 2310 numbered asteroids in the region, I then compared my results with those of the AstDyS site. I used the method described in Knežević & Milani (2000) applied to the results of my numerical simulation described in Section 2 for the 2310 objects that survived the simulation and have less than 'pathological' values of errors in proper elements. Planetary frequencies were discarded in the Fourier spectra of the equinoctial elements in order to obtain the values of proper g and s. Using the errors in proper $a, \sin i, n, g$ and s given at the AstDyS site, I verified for which objects the values of proper elements were outside the limits $\mathrm{el} - \sigma_{\mathrm{el}}$, $\mathrm{el} + \sigma_{\mathrm{el}}$, where 'el' is one of the five elements in the catalogue. According to this criterion, I found no discrepancy between the values of proper $a, e, \sin i, n$ and s from the AstDyS site and those obtained with my simulations. 26 objects (1.12 per cent of the total) have discrepancies in the values of proper eccentricities. All of these objects are objects either with very low values of proper eccentricity or strongly perturbed by secular resonances, and since, as discussed by Knežević & Milani (2000), these cases have large errors in proper eccentricities for reasons discussed in Section 2, I believe that the discrepancies are understandable.

More important are the discrepancies in the values of proper g, especially for the members of the Hansa family with $e_{\mathrm{proper}} < 0.0179$ (Carruba & Michtchenko 2009). For these objects, the ϖ angle in the (h, k) plane does not describe a full circle, and this yields negative values of the precession frequency g when the method of Knežević & Milani (2000) is applied, as described by the authors. 368 asteroids (15.93 per cent of the total, including the 26 asteroids with discrepancies in the values of proper eccentricities) have discrepancies between the AstDyS values of g and mine. Fig. 5 displays an (e, g) projection of (a) AstDyS asteroids and (b) my results in the region of the Pallas and Hansa families. As can be seen in the figure, the tail of objects with very retrograde values of proper g present in the Hansa family in the AstDyS catalogue is now removed in my own set of proper elements.

I have thus finally verified how many of the 1475 objects that had 'stable values' of proper elements in the AstDyS site were stable in my run and all of them were also found to be stable according to my simulations, stating a good agreement between the two methods.

Based on this result, I believe that it seems safe to use proper elements obtained with the results of numerical simulations, at least

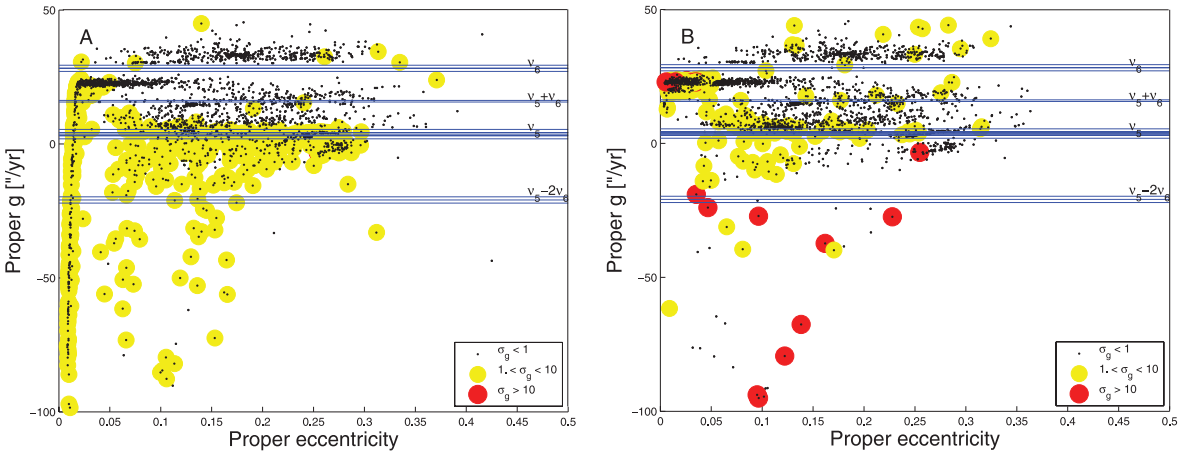

Figure 5. (a) An (e, g) projection of AstDyS asteroids in the region of the Pallas and Hansa families. Small full dots display asteroids with standard deviation in σ_g between 1 and 5, while large full dots show asteroids with σ_g larger than 5. (b) An (e, g) projection of the results of my simulation.

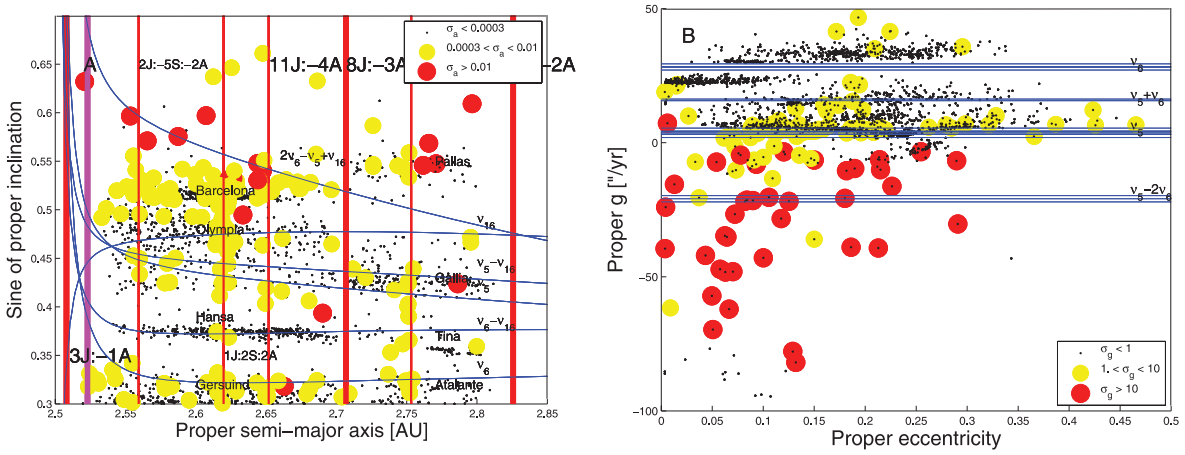

Figure 6. (a) (a, $\sin i$) and (b) (e, g) projections of the synthetic proper elements and frequencies obtained for 2142 multi-opposition asteroids in the region of the Pallas and Hansa families.

with regard to proper semi-major axis, inclination and frequency of precession of the node. Caution should be used when dealing with proper eccentricity and, in greater part, the frequency of pericentre precession. This has a particular importance regarding families obtained in the space of proper frequencies. The problems associated with the inevitable uncertainties in the values of g when family determination is concerned will be discussed in Section 3.

Finally, now that the procedure for obtaining proper elements is calibrated, I have used this method to obtain proper elements for 4320 multi-opposition objects in the region. At the end of the 10-Myr simulation, 4173 objects survived the simulation and had less than 'pathological' values of errors in proper elements. Of these, 2142 objects had proper elements that are in the region of the Pallas and Hansa families, i.e. between the 3J:–1A and 5J:–2A mean-motion resonances and with $\sin i > 0.3$.

Fig. 6 shows (a) (a, $\sin i$) and (b) (e, g) projections of the synthetic proper elements and frequencies obtained for 2142 multi-opposition asteroids in the region of the Pallas and Hansa families. As can be seen in the figure, the distribution of proper elements is quite similar to that of the numbered objects in the region (see Fig. 2b and Fig. 5b), thus confirming the validity of the approach used to obtain proper elements for multi-opposition objects.

3 DYNAMICAL FAMILIES AND CLUMPS IN THE PALLAS AND HANSA REGION

Now that I have obtained a reliable set of proper elements for both numbered and multi-opposition asteroids in the region of the Pallas and Hansa families, the next logical step is to identify dynamical families and clumps in the region.

In identifying asteroid families in the space of proper elements, two parameters are fundamental: the cut-off distance at which the family members are defined, d_0, and the minimum number of objects $N_{\rm min}$ for a cluster to be considered significant. Beaugé & Roig (2001) define a nominal distance cut-off as the average minimum distance between all neighbouring asteroids in the same region of the asteroid belt. The value of $N_{\rm min}$ is defined by Zappalà et al. (1995) as

$$N_{\rm min} = N_0 + 2\sqrt{N_0}, \qquad (1)$$

where N_0 is the average number of orbits within a sphere of radius d_0 at every point of the proper-element space. A cluster with a number of objects larger than this critical value is called a clump, while a family is a cluster with a number of members larger than $2.5N_{\rm min}$. As I shall discuss in more detail in Section 9, the region of the Pallas and Hansa families is delimited by the 3J:–1A and 5J:–2A mean-motion resonances in proper a and by the ν_6 secular resonance at low inclination. The nominal distance velocity cut-off as defined in Beaugé & Roig (2001) is 139.33 m s^{-1} for all 2310 numbered objects in the region and 116.92 m s^{-1} for all 4452 numbered and multi-opposition asteroids in the area. Fig. 7 displays the average number N_0, $N_{\rm min}$ and the maximum number max (N_i) of asteroids as a function of the velocity cut-off, for (a) numbered and (b) all asteroids in the region. The value of $N_{\rm min}$ corresponding to $d_0 = 139.33$ m s^{-1} is 8, while the value of $N_{\rm min}$ corresponding to $d_0 = 116.92$ m s^{-1} is 11. As can be seen in Fig. 7, the fact that max (N_i) is much larger than $N_{\rm min}$ may be a hint that background objects are more numerous than family ones, in contrast to what happens in the Phocaea family region (Carruba 2009). Note that in the larger sample that includes multi-opposition objects, while the max (N_i) of asteroids as a function of the velocity cut-off is significantly larger than the case with just numbered asteroids, the values of N_0 and $N_{\rm min}$ only increase slightly. This is also observed in the domain of proper frequencies, as discussed later in this section.

Regarding the domain of proper frequencies, following the approach of Carruba & Michtchenko (2007) I determined the families with a metric of the form

$$f = \sqrt{h_1 \left(\frac{\Delta n}{h_0}\right)^2 + h_2(\Delta g)^2 + h_3[\Delta(g+s)]^2}, \qquad (2)$$

where $h_1 = h_2 = h_3 = 1$. I determined the nominal frequency cut-off, defined as the average minimum distance between all neighbouring asteroids in the (n, g, $g + s$) domain, and found a value of $f_0 = 0.6273$ arcsec yr^{-1} for numbered objects and $f_0 = 0.5145$ arcsec yr^{-1} for all asteroids in the region. Fig. 7 also displays the average number N_0, $N_{\rm min}$ and the maximum number max(N_i) of asteroids as a function of the frequency cut-off defined by equation (2) for (c) numbered and (d) all objects in the region. The value of $N_{\rm min}$ corresponding to $f_0 = 0.6273$ arcsec yr^{-1} is 15, while the value corresponding to $f_0 = 0.5145$ arcsec yr^{-1} is 17. As observed for the values of $N_{\rm min}$ and max N_i obtained in the proper-element domain, in the domain of frequencies I still observe a much larger value of max N_i with respect to $N_{\rm min}$. Again, this may suggest that the local background of the Pallas and Hansa families is indeed

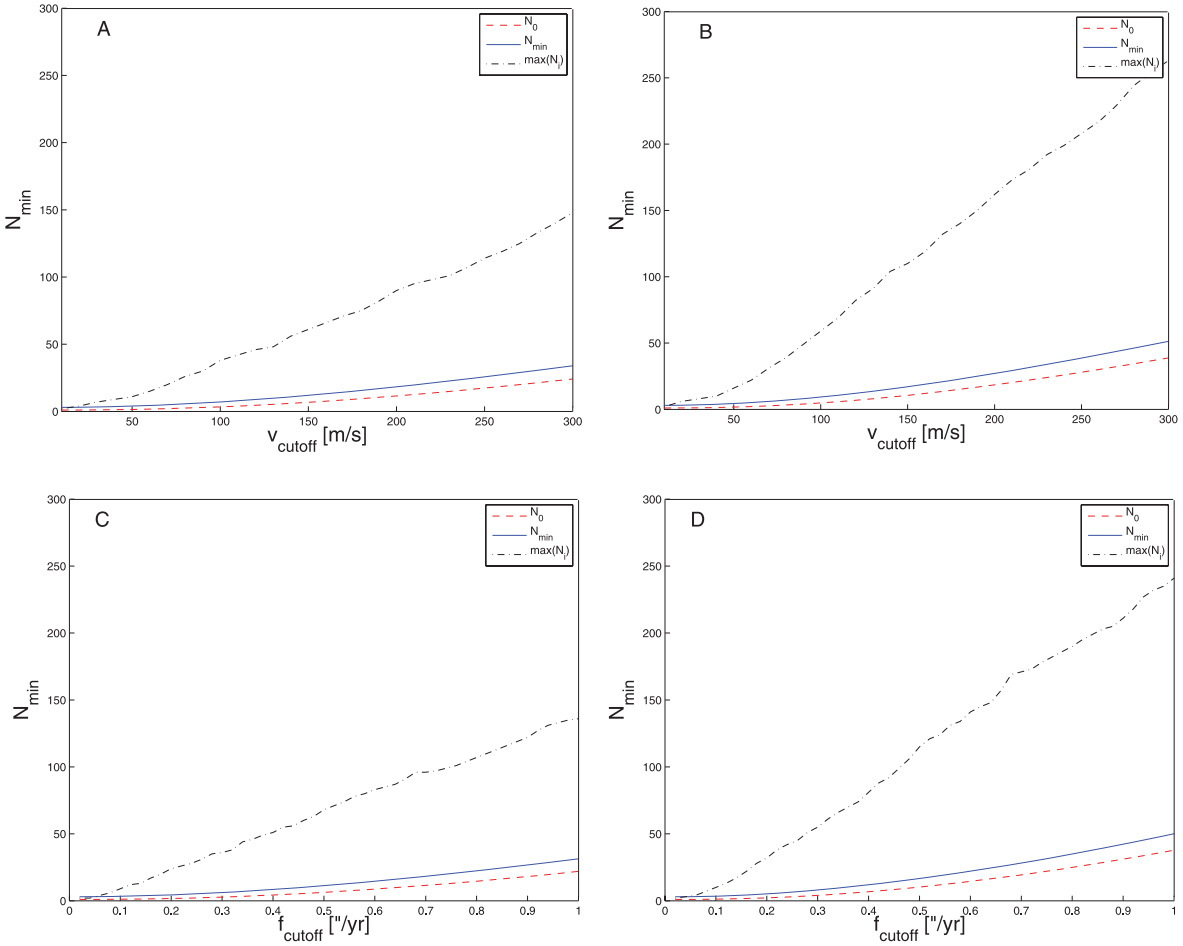

Figure 7. The average number $N_0, N_{\rm min}$ and the maximum number max(N_i) of asteroids as a function of the velocity cut-off for (a) numbered and (b) all asteroids in the region of the Pallas and Hansa families. (c) and (d) display the same numbers as a function of the frequency cut-off.

dominated by background objects, rather than by family ones, in contrast to the case of the Phocaea family (Carruba 2009).

The next logical step was to obtain dynamical families and clumps in the eight regions in the (a, sin i) plane defined in Section 2.1. Here I followed the same procedure used in Carruba (2009) to obtain families and clumps in spaces of both proper elements and proper frequencies for the region of the Phocaea family. Fig. 8 displays the procedure used for the Gallia family region; analogous results for the other seven regions will not be shown for the sake of brevity, but are available upon request to the author.

The Gallia clump of Gil-Hutton (2006) dominates the Gallia area, so I started by obtaining the dynamical family in the domain of proper elements (a, e, sin i) associated with this asteroid. Fig. 8(a) displays the number and differential number of the classical Gallia family as a function of the cut-off. For a cut-off of 224 m s^{-1} the family merges with the (40134) clump, while for a cut-off of 277 m s^{-1} the family joins the local background. The vertical line shows the nominal distance velocity cut-off d_0. Here I choose to work with a slightly larger value of d_0 (122 m s^{-1}) rather than the one found earlier of 116.92 m s^{-1}, in order to account for the behaviour of the highly inclined Pallas and Barcelona families, which merge with substructures (such as the (531) clump for the case of the Pallas family) for $d_0 = 121$ m s^{-1}. At this cut-off, a clump must have at least 12 members and a family 30 members.

To re-identify asteroid families I also constructed a stalactite diagram in the traditional way defined by Zappalà et al. (1990) and Brož & Vokrouhlický (2008): I started with (148) Gallia as the first central body and identified all the bodies associated with it at $d_{\rm cut-off} = 280$ m s^{-1}, a value for which no other independent cluster of asteroids was found. I then decreased the cut-off and identified the families and clumps among the asteroids not associated with (148) Gallia. Fig. 8(b) displays my results in the interval of cut-offs between 85 and 285 m s^{-1}. Full black squares are associated with families in the region, and empty black squares are associated with clumps, according to the limits displayed in Fig. 7. The (40134) clump is quite visible in the stalactite diagram and satisfies the criteria defined in Carruba (2009) for the identification of a clump: the clusters should be observable for a cut-off equal to d_0 and the 'length' of the 'stalactite' associated with the family should be at least 20 per cent of d_0, i.e. $\simeq$25 m s^{-1}.

I then repeated the same procedure using the frequency hierarchical clustering method (FHCM) in the (n, g, $g + s$) domain and Fig. 8(c) and (d) display the results in this domain. Again, the f_0 value that I used to work with was larger than the nominal one (0.605 arcsec yr^{-1} rather than 0.5145 arcsec yr^{-1}), to account for the behaviour of the Pallas and Barcelona families. At this cut-off a clump must have at least 22 members and a family 55 members. One may notice that the (40134) clump is no longer observable at a frequency cut-off equal to f_0 (but it is still detectable at larger cut-offs) and it is not therefore listed as a real dynamical group. Also, the frequency family at the 0.605 arcsec yr^{-1} cut-off connects to (71) Niobe, and should therefore called the Niobe family (for the

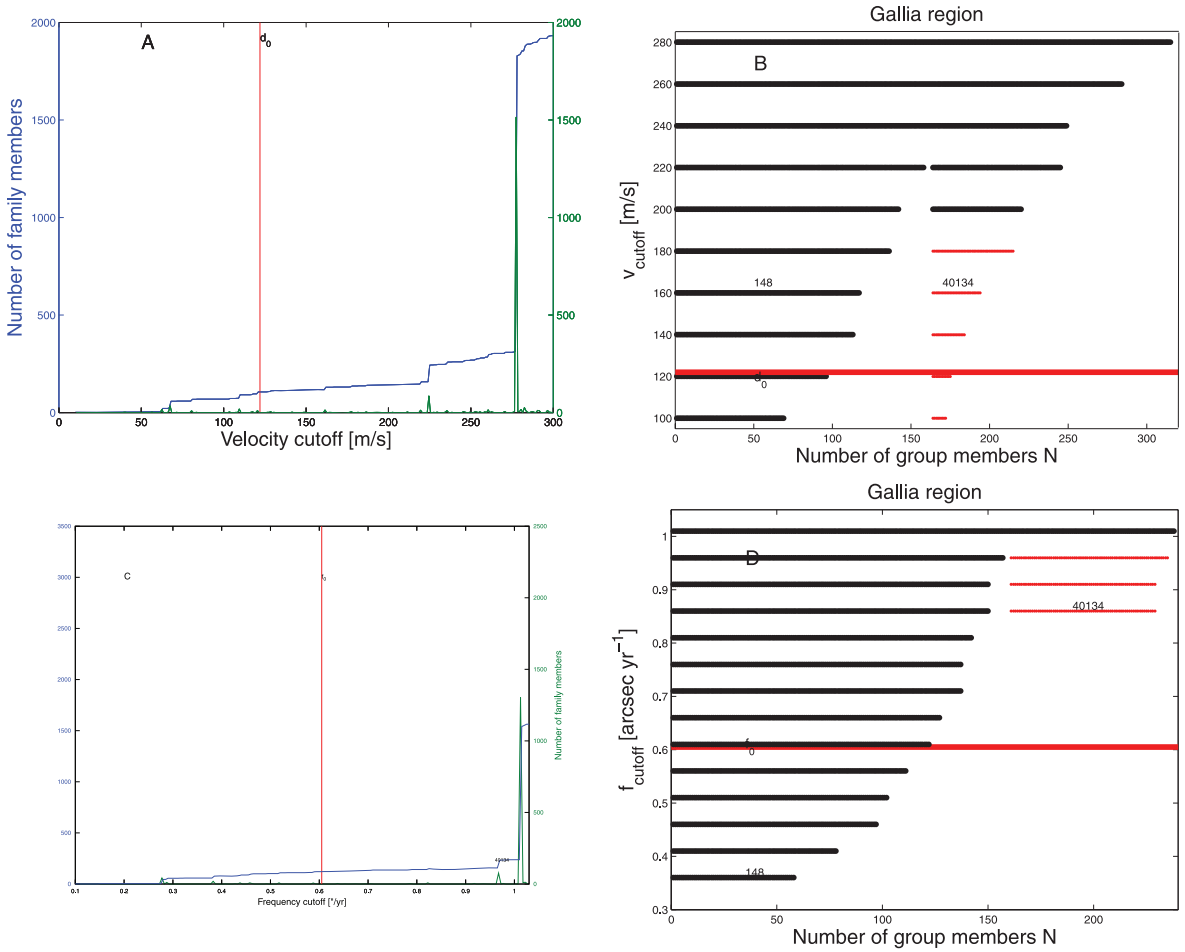

Figure 8. (a) The number and differential number of the classical Gallia family as a function of cut-off. The number at the peak of the differential number of family members is related to the (40134) clump that was englobed by the Gallia family at the higher velocity cut-off. (b) A stalactite diagram of the Gallia family region. (c) and (d) The same as (a) and (b), but for frequency groups in the (n, g, $g + s$) domain.

sake of simplicity, I will keep the Gallia name for the frequency family as well).

Table 1 summarizes the results of the search for families and clumps in the Pallas and Hansa regions. In the first column I report whether the group is a family or a clump; the letters 'c' or 'f' identify whether the family was found in the space of proper elements or proper frequencies. The second column reports the lowest numbered member of the group, while the third column shows the number of objects in the group. The fourth column displays how many objects in the group have 'stable' proper elements, i.e. with 'small errors' as defined in Section 2.1. Families with a larger proportion of objects with stable proper elements can be considered more reliable. Finally the fifth and sixth columns report the number of group members for which either spectral or SDSS-MOC3 information is available, respectively.

Here I will briefly discuss my findings in the eight regions in the (a, sin i) plane introduced in Section 2.1. In the region of Barcelona, the Barcelona clump of Gil-Hutton (2006) is now a family of 540 members in the proper-element domain, and of 550 members in the proper-frequency domain. Only five (0.9 per cent of the total) of the classical members have stable proper elements, while only three (0.5 per cent of the total) of the frequency ones have reliable proper elements, which seems to indicate that the family is in a region of highly unstable proper elements, possibly caused by its proximity to the ν_{16} secular resonance. A low-eccentricity clump around (208080) 1999 VV180 with 11 members, none which has stable proper elements, was identified in the proper-element domain but not in the proper-frequency one. The statistical significance of this clump should be further investigated with the method used for minor clumps in the Phocaea regions in Carruba (2010).

In the Olympia region I could not find any family in the space of proper elements, but five clumps were identifiable: (4203) Brucato, 12 members, none with stable proper elements; (18511) 1996 SH4, 12 members, none with stable proper elements; (36240) 1999 VN44, 11 members, one of which has stable proper elements; (70280) 1999 RA111, 14 members, all with unstable proper elements; (75938) 2000 CO80, 13 members, five of which have stable proper elements. The (4203) Brucato clump becomes a family with 249 members (14 of which have stable proper elements) and the (36240) 1999 VN44 clump is also visible in the proper-frequency domain, with 46 members. The other clumps observed in the proper-element domain are substructures of the (4203) Brucato family in the frequency domain.

The new proper elements obtained for the Hansa region permit a solution of the problem observed with the g frequency when the AstDyS data were used to obtain frequency families (Carruba & Michtchenko 2009). As discussed in Section 2, asteroids with values of forced eccentricities larger than the free one, such as is

Table 1. Families and clumps in the region of the Pallas and Hansa families.

ID	Name	N	$N_{\rm stable}$	$N_{\rm spec}$	$N_{\rm SDSS-MOC3}$
Family(c)	(945) Barcelona	540	5	1	10
Clump(c)	(208080) 1999 VV180	11	0	0	0
Family(f)	(945) Barcelona	550	3	1	12
Clump(c)	(4203) Brucato	12	0	0	0
Clump(c)	(18511) 1996 SH4	12	0	0	0
Clump(c)	(36240) 1999 VN44	11	1	0	1
Clump(c)	(70280) 1999 RA111	14	0	0	1
Clump(c)	(75938) 2000 CO80	13	5	0	1
Family(f)	(4203) Brucato	249	14	0	17
Clump(f)	(36240) 1999 VN44	46	10	0	5
Family(c)	(480) Hansa	859	201	3	0
Clump(c)	(33969) 2000 NM13	21	11	0	5
Family(f)	(480) Hansa	888	203	2	0
Clump(f)	(82426) 2001 NB20	24	1	0	1
Family(c)	(686) Gersuind	151	125	2	6
Family(f)	(686) Gersuind	174	143	2	10
Family(c)	(2) Pallas	35	33	5	3
Family(f)	(2) Pallas	79	71	6	5
Family(c)	(148) Gallia	106	100	1	5
Family(f)	(148) Gallia	121	106	2	6
Clump(c)	(40134) 1998 QO53	16	11	0	1
Family(c)	(1222) Tina	72	8	1	5
Family(f)	(1222) Tina	86	10	1	6

the case for (480) Hansa, may show retrograde values of proper frequency g when the Knežević & Milani (2000) approach to synthetic proper elements is used. The new synthetic proper elements used here allow identification of the Hansa family in the frequency domain (n, g, $g + s$) without the problems observed in Carruba & Michtchenko (2009).[4] The Hansa family in the proper-element domain had 859 members, 658 of which have stable proper elements. The new Hansa family in the frequency domain had 888 elements (685 with stable proper elements), without the need to perform any regularization such as the one described in Carruba & Michtchenko (2009). The fact that the number of frequency-family members is now comparable to the number of classical-family members without any regularization seems to confirm, in my opinion, the validity of the approach used to obtain synthetic proper elements in this paper. A clump around (33969) 2000 NM13 with 21 members found in the proper-element domain and one around (82426) 2001 NB20 with 24 members identified in the frequency domain were also encountered in the region.

In the region of Gersuind, the former Gil-Hutton (2006) family of (686) Gersuind with 28 members now has 151 members in the proper-element domain and 174 members in the frequency domain. Both families are characterized by a large proportion of members with stable elements (125 and 143, respectively).

No independent clump was observed in the region of the Pallas family but, as discussed earlier, the classical clump around (531) Zerlina merges with the Pallas family only for a cut-off of $d_0 = 121\,{\rm m\,s^{-1}}$, while the frequency clump around (3579) Rockholt merges with the Pallas frequency family for a cut-off of $f_0 = 0.600\,{\rm arcsec\,yr^{-1}}$, which motivated, along with similar considerations for the Barcelona family, my choice of cut-offs.

[4] To avoid the problem associated with the large errors in proper frequencies of (480) Hansa, as in Carruba & Michtchenko (2009) I used (40971) 1999 TY264 as the central body of the family.

The situation of groups in the Gallia region was already discussed earlier in this section, and no group was found in the Atalante region. More interesting is the situation of the Tina region, where a new family around (1222) Tina was found in both proper-element (72 members) and frequency (86 members) domains. The new family is characterized, as are families in the Barcelona and Olympia region, by the predominance of asteroids with unstable elements and by a large number of multi-opposition members (more than 60 per cent of the family members are objects with proper elements obtained for the first time in this work).

Fig. 9 displays contour plots of the number density of asteroids (see Carruba 2009 for a description of the procedure used to generate such plots; here I have used 33 steps of 0.02 au in a and 38 steps of 0.016 in $\sin i$) in the (a, $\sin i$) representative plane. Higher number densities of objects are shown in whiter tones. Following the example of Michtchenko et al. (2010), I divided my population of objects into small-eccentricity bodies ($e < 0.175$) and large-eccentricity ones ($e > 0.175$).

Fig. 9 displays density maps in the (a, $\sin i$) representative plane for (a) small-eccentricity bodies and classical groups, (b) small-eccentricity bodies and frequency groups, (c) large-eccentricity bodies and classical groups and (d) large-eccentricity bodies and frequency groups. Family members are shown as asterisks, while clump members are displayed as small circles. The effect of the linear secular resonances ν_5, ν_6, ν_{16} in removing the observed population of asteroids is quite clear in the density maps.

Among the differences between classical and frequency families, one may observe the presence of the Brucato family, observable in the (n, g, $g + s$) domain at low eccentricities but visible only as a clump in the (a, e, $\sin i$) space. At large eccentricities one may observe that the Pallas family is more extended in semi-major axis in the frequency domain than in the proper-element one. One may also notice the absence of the (40134) clump in the frequency domain; this is retrievable only for larger values of the cut-off than the one used.

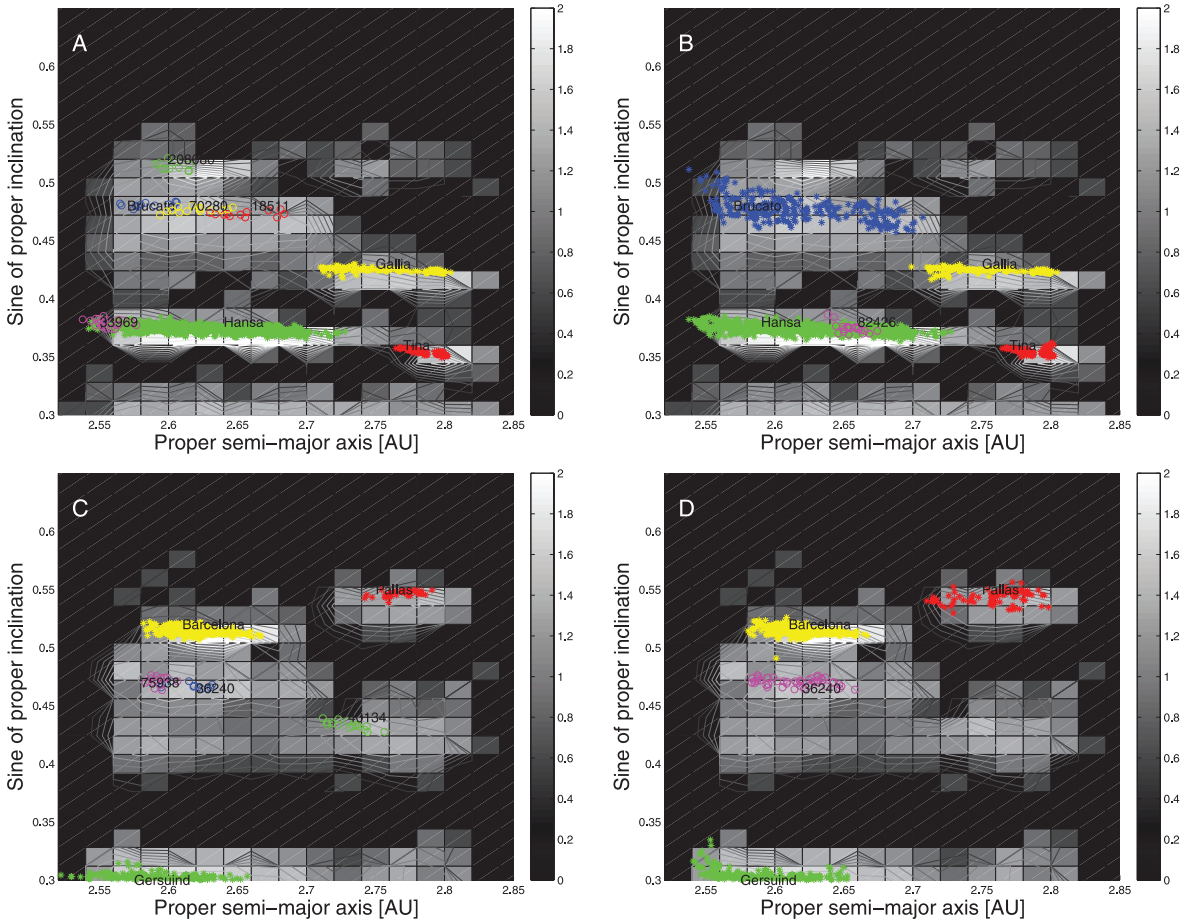

Figure 9. Density maps in the (a, sin i) representative plane for (a) small-eccentricity bodies and classical groups, (b) small-eccentricity bodies and frequency groups, (c) large-eccentricity bodies and classical groups and (d) large-eccentricity bodies and frequency groups.

To conclude, four new dynamical families (five if we include the Brucato frequency family) were discovered in this work: Gersuind, Barcelona, Gallia and Tina (the last was not known even as a clump in any previous work). Understanding whether these new families are the product of real collisional events will require an analysis of the taxonomy and properties of their members. I will concentrate my attention on these issues in the next sections. In the next subsection I will discuss family subgroups and asteroid pairs in the region.

3.1 Family subgroups and asteroid pairs

As a subproduct of the process of family determination, I obtained a few subgroups inside some of the families in the region. Table 2 displays the identification of the lowest numbered object in the subgroup, the name of the family to which it belongs ('c' identifies classical families, 'f' frequency ones) and the cut-off for which it merges with the family. Subgroups were identified for cut-offs larger than 100 m s^{-1} in proper-element space and greater than 0.400 arcsec yr^{-1} in frequency space. I refer the reader to Section 3 for a more in-depth discussion of the subgroups reported in Table 2.

Table 2. Subgroups in the region of the Pallas and Hansa families.

ID	Family	Cut-off
18511	Brucato(f)	0.500 arcsec yr^{-1}
70280	Brucato(f)	0.550 arcsec yr^{-1}
75938	Brucato(f)	0.575 arcsec yr^{-1}
6894	Hansa(c)	118 m s^{-1}
33167	Hansa(c)	119 m s^{-1}
531	Pallas(c)	119 m s^{-1}
3579	Pallas(f)	0.605 arcsec yr^{-1}

Also, recently Pravec & Vokrouhlický (2009) and Milani et al. (2010) looked for asteroid pairs in the main belt. These are objects that are extremely close in proper-element space and could be associated with double asteroids that recently split up. The first of the filters used by Milani et al. (2010) required asteroid pairs to be less distant in proper-element space by a distance of 4.2×10^{-4}, defined by the metric

$$d_{\rm p} = \sqrt{\frac{5}{4}\left(\frac{\delta a}{a_{\rm p}}\right)^2 + 2\delta e_{\rm p} + 2\delta I_{\rm p}}, \qquad (3)$$

where δ refers to the difference in proper elements between the parent body and the possible lost satellite. This distance corresponds to a distance of 9 m s^{-1} using the standard metric of Zappalà et al. (1995). Table 3 shows the 12 possible asteroid pairs identified in this work in increasing order of distance according to the metric given in equation (3) (for simplicity, distances are given using the standard metric of Zappalá et al. 1990). Here I only considered pairs with stable proper elements. Nine more pairs with one or both asteroids having unstable proper elements were also identified, but will not be given in this work.

Table 3. Candidates for past asteroid pairs in the region of the Pallas and Hansa families.

ID_1	ID_2	d (m s^{-1})
61728	216855	4.08
151802	2003 XO10	4.80
2001 XF16	2008 AD10	6.22
116053	146455	6.45
2006 UO5	2001 XG19	6.69
195451	2003 EB42	6.82
61226	95694	7.15
40853	114820	7.58
42800	110201	8.21
54896	70610	8.45
20949	2003 UA15	8.49
5438	208099	8.54

I should emphasize that further study is needed on the nature of these objects, since only the first filter of Milani et al. (2010) was applied here. The confirmation of these pair candidates as possible past broken couples should be considered as a possible line of research for future works.

4 THE COMPOSITIONAL ANALYSIS

As a preliminary step in the analysis of the local dynamical groups, I reviewed current knowledge about the taxonomical classification of members of the families and clumps in the region using the data present in three major photometric/spectroscopic surveys: the Eight-Color Asteroid Analysis Survey (ECAS: Zellner, Tholen & Tedesco 1985; Tholen 1989), the Small Main Belt Spectroscopic Survey (SMASS: Xu et al. 1995; Bus & Binzel 2002a,b) and the Small Solar System Objects Spectroscopic Survey (S3OS2: Lazzaro et al. 2004). I identified in the region of the Pallas and Hansa families two A-type, one L-type, 10 S-type, 10 X-type, 14 C-type, six B-type and one D-T-type object. Table 1 reports in the fifth column the number of group members with spectral identification.

Gil-Hutton (2006) reported that of the five members with spectral identification in the Pallas classical family four were B-type asteroids while one, (4969), was a C-type object and probably an interloper. The only two objects with spectral identification in the Hansa family were both S type, while in the Gersuind family one object, (686) Gersuind, was an S-type while (1609) was a D-type asteroid.

With respect to the work of Gil-Hutton (2006), I found that no taxonomical information is available on any of the clumps that I found in this work and very little is available for the families. The only object with spectral classification in the Barcelona family is (945) Barcelona, which is Sq type. No information is available for the groups in the Olympia region, while for the Hansa family three asteroid members of the classical family (480, 925 and 4880; 480 is not a member of the frequency family) are all S-type. I confirmed the two asteroids with spectral identification in the Gersuind family, and I found seven objects with spectral identification in the Pallas families (one of these, 5222, did not survive the length of my integration so that synthetic proper elements are not available for this object). Five of these objects, 2, 531, 2382, 3579 and 5234, are B-type, which seems to confirm the possibility of the Pallas family being a B-type group, but two family members, 1301 and 4969, are C-type, which undermines this possibility. The paucity of data on this family does not allow one to make a stringent conclusion on the family taxonomy. In the Gallia family one object, 148, is

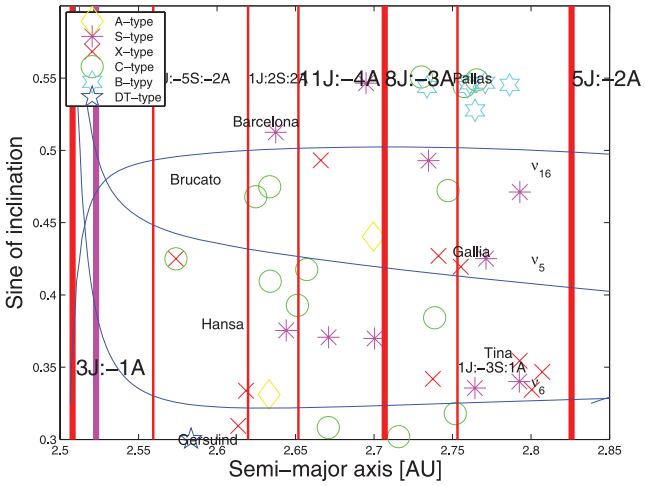

Figure 10. Taxonomic distribution of asteroids in the region of the Pallas and Hansa families.

S-type, while a member of the frequency family, 71 Niobe, is X-type. Finally, (1222) Tina is the only family member with a spectral classification (X-type).

Overall, with the possible exception of the Hansa and Pallas families, spectroscopic data are not enough to allow any stringent conclusions regarding any of the groups encountered in this work. Fig. 10, which shows an (a, sin i) projection of asteroids in the region with known spectral types, summarizes the results of my discussion. As can be seen in the figure, with the possible exception of the Hansa and Pallas family regions no area is taxonomically 'pure', with the predominance of a single spectral type. Further information is therefore needed before conclusions on the taxonomical validity of the groups found in this work can be confirmed.

For the purpose of extending the sample for which information on taxonomy is available, I turn my attention to SDSS-MOC3 data. The Sloan Digital Sky Survey Moving Object Catalog, denoted SDSS-MOC3 (3 stands for the third release, here I am using the third release rather than the fourth because of the better signal-to-noise ratio for the fluxes in that release), lists astrometric and photometric data for asteroids observed by the 2.5-m Sloan telescope located at Apache Point Observatory in Sunspot, New Mexico. To date (fourth release), the survey has determined positions, brightnesses and five-colour CCD photometry of 471 569 moving objects (Parker et al. 2008).

The flux reflected by the detected objects was measured almost simultaneously in five bands (measurements in two successive bands were separated in time by 72 s) with effective wavelengths 3557 Å (u band), 4825 Å (g band), 6261 Å (r band), 7672 Å (i band) and 9097 Å (z band), and with 0.1–0.3 μm bandwidths (Fukugita et al. 1996). Here I follow the approach of Roig and Gil-Hutton (2006) to obtain principal components in the space of albedos F_u, F_g, F_i, F_z. Using the criteria introduced by Roig & Gil-Hutton (2006) to reject data with large errors, I obtain a data set of 252 numbered objects with SDSS-MOC3 data in the Pallas and Hansa family regions.

Once the two first principal components are found, the data can be used to classify asteroids according to their taxonomic types and to determine asteroid families in the space of proper elements and colours simultaneously. The SDSS-MOC3 principal-component criteria are not of course a conclusive proof that an asteroid belongs to a given taxonomical class, but may furnish

precious hints on objects, such as V-type asteroids, for which no spectral information is available (Roig & Gil-Hutton 2006)).

Bus & Binzel (2002a,b) and Nesvorný et al. (2005) introduced the following extended metric in the space of proper elements and colours:

$$d_3 = \sqrt{d^2 + C_{PC}[(\delta PC_1)^2 + (\delta PC_2)^2]}, \quad (4)$$

where d is the distance given by the standard metric of Zappalá et al. (1990) and PC_1 and PC_2 are the two first principal components. Carruba & Michtchenko (2007, equation 3) also introduced a metric of colours and frequencies in the $(n, g, g + s, PC_1, PC_2)$ domain of the form

$$d_4 = \sqrt{f^2 + D_{PC}[(\Delta PC_1)^2 + (\Delta PC_2)^2]}, \quad (5)$$

where f is the standard distance metric in the $(n, g, g + s)$ frequency domain (Carruba & Michtchenko 2007) and D_{PC} is a numerical factor, empirically set equal to 200 to give comparable results for the typical differences in proper frequencies and those in principal components.

Following the approach of Carruba & Michtchenko (2007), I selected as first member of the colour groups one asteroid with principal-component data for each of the groups for which at least one member has SDSS-MOC3 data. I start my analysis by using the distance metric of principal components and proper elements. For a cut-off of 390 m s^{-1} the 33969 clump coalesces with asteroids in the local background of the Hansa family, so I decided to work with a cut-off of 385 m s^{-1}, which is in agreement with similar values found for the region of the Phocaea family (Carruba 2009). At this cut-off the Barcelona family has six members, five of them with principal components compatible with an Sq taxonomical class (see Fig. 11(a) and also Nesvorný et al. (2005) for the location of Sq asteroids in the principal-component plane), thus confirming the possible identification of Barcelona as an Sq-type family.

All the minor clumps found in the space of proper elements only have one or two members in the space of proper elements and colours, which is not enough to give information on their taxonomy. Most of them are compatible with an S-type class, but the 70280 and 33969 clumps also show the presence of SDSS-MOC3 objects compatible with X and C compositions. No member of the Hansa family was found in the SDSS-MOC3 catalogue, so it was not possible to obtain this family in the space of proper elements and colours, but most of the asteroids in the family local background are compatible with an S-type class, which seems to reinforce the information obtained from the spectral data of the family members. All seven members of the Gersuind family are in the region of the S-type complex, and no D–T asteroid was observed. This may suggest that the (1609) D–T asteroid in the Gersuind family may be an interloper. The Pallas family has two members that are compatible with either the B- or C-type class. Gallia has five S-type-compatible members, while Tina has two S-type objects. Overall, with the exception of the Pallas family and, possibly, the 70280 and 33969 clumps, the region seems to be dominated by S-type objects, but further study is needed to confirm this statement. Fig. 11(b) shows an $(a, \sin i)$ projection of the families with more than one object found in the space of proper elements and colours, which summarizes my results.

I then turned my attention to the domain of proper frequencies $(n, g, g + s)$ and colours. At a cut-off of 2.4 arcsec yr^{-1}, the 84646 frequency clump coalesces with asteroids in the local background of the Hansa family, so I decided to work with a cut-off of 2.3 arcsec yr^{-1} , which is in agreement with similar values found for the region of the Phocaea family (Carruba 2009). At this cut-off the Barcelona family has four members, all with principal components compatible with an Sq taxonomical class (see Fig. 12a), further confirming the possible identification of the Barcelona group as an Sq-type family.

The two frequency clumps around (36240) and (84646) all have one S-type member in the space of proper frequencies and colours. The Brucato frequency family has five members, almost equally divided between the C and X complexes. The Gersuind family has seven members, all in the S complex. The Pallas family has one member in the C complex and Gallia is characterized by four members in the S complex. Finally, the Tina family has one member in the S complex.

Overall, colour–frequency groups seems to confirm the findings for the colour–element groups. The Brucato frequency family, which englobes the 70280 classical clump, is characterized by the presence of both C- and X-type compatible objects, which seems to put in doubt the viability of the group as the product of a collisional event. Fig. 12(b) shows an $(a, \sin i)$ projection of the families with more than one object found in the space of proper frequencies and colours, which summarizes my results.

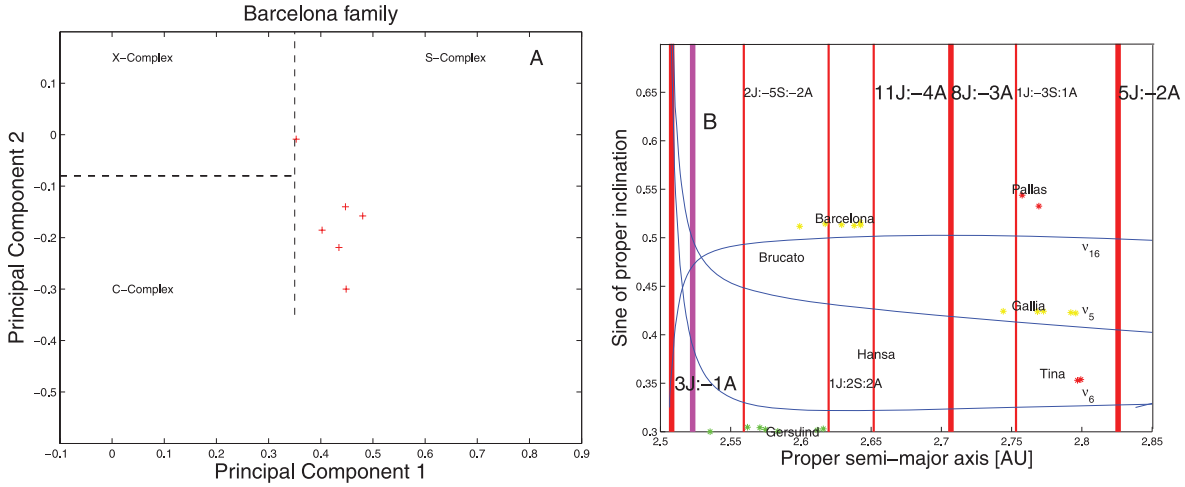

Figure 11. (a) The location in the principal-component (P_1, P_2) plane of the six members of the Barcelona colour–element family. (b) An $(a, \sin i)$ projection of families in the space of proper elements and colours.

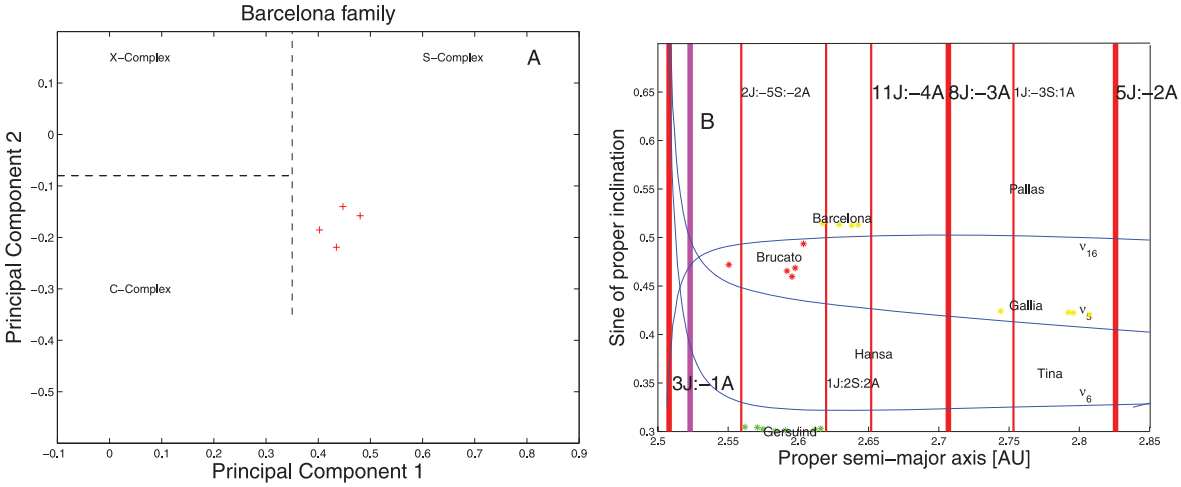

Figure 12. (a) The location in the principal-component (P_1, P_2) plane of the six members of the Barcelona colour–frequency family. (b) An (a, sin i) projection of groups in the space of proper frequencies and colours.

In the next section I will investigate the values of albedos and absolute magnitude for asteroids in the region that are available in the literature.

5 GEOMETRIC ALBEDOS AND ABSOLUTE MAGNITUDES

The cumulative size distribution of asteroid family members can be used to obtain important information about the collisional and orbital evolution of asteroid families (Vokrouhlický et al. 2006b). Estimates of the asteroid diameters can be obtained via the relationship

$$D = \frac{D_0}{\sqrt{p_V}} \times 10^{-0.2H}, \quad (6)$$

where $D_0 = 1329$ km, H is the asteroid absolute magnitude and p_V is the geometric albedo. To obtain reliable estimates of the diameters of asteroids, it is therefore important to first obtain good values of the geometric albedos and absolute magnitudes of the asteroids. Regarding asteroid albedos, I turn my attention to the work of Tedesco et al. (2002), which reported values of geometric albedo (with their uncertainties) for 2226 bodies. Of these, I found 43 objects in the region of the Pallas and Hansa families for which synthetic proper elements were also available. Eight of these objects belongs to either classical or frequency families and have a reported spectral classification.

Fig. 13(a) displays an (a, sin i) projection of the 43 objects with albedos in the region. Asteroids with albedos lower than 0.10 (usually associated with C-type bodies) are displayed with small black dots, those with albedos between 0.10 and 0.25 (associated with S-type objects, Bus & Binzel 2002a,b) are shown with medium full dots and asteroids with albedos larger than 0.25 are displayed with large full dots. As can be seen in the figure, low- and high-albedo objects are pretty much mixed, especially in the Olympia region, with the Brucato frequency family showing relatively low values of albedos, compatible with the C-complex membership of some of its members. The Barcelona and Gersuind families are characterized by values of albedos compatible with S-type composition, while the high value of albedo of the Gallia family is due to the fact that the only object with albedo data in the family, (71) Niobe, is probably an interloper. Overall, a slight majority of objects in the region have low-albedo values, 44 per cent of objects have albedos in the S-type range and only three objects have large albedo values. The

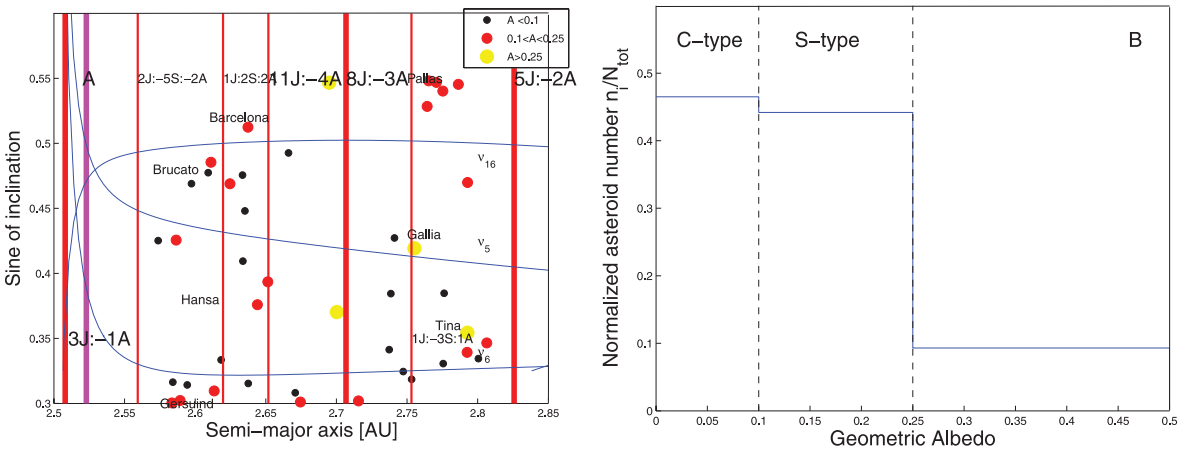

Figure 13. (a) An (a, sin i) projection of the orbital location of asteroids for which a value of the geometric albedo is available in the region of the Pallas and Hansa families. (b) Histogram of the normalized number of objects per unit bin in the albedo intervals 0.00–0.10 (C-type), 0.10–0.25 (S-type) and larger than 0.25, for all asteroids in the region (solid line).

Table 4. Mean value of the albedo for families in the region of the Pallas and Hansa families.

ID	Name	p_V	σp_V	$N_{\rm albedo}$
Family(c,f)	(945) Barcelona	0.2416	0.024	1
Family(f)	(4203) Brucato	0.0838	0.044	2
Family(c,f)	(686) Gersuind	0.1282	0.030	2
Family(c,f)	(2) Pallas	0.1560	0.009	3
Family(c,f)	(148) Gallia	0.3052	0.013	1
family(c,f)	(1222) Tina	0.3086	0.059	1

situation is summarized in Fig. 13(b), which shows a histogram of the normalized number of objects per unit bin in the albedo intervals 0.00–0.10 (C-type), 0.10–0.25 (S-type) and larger than 0.25, for all asteroids in the region (blue line).

Table 4 displays values of the mean albedo for the families for which such data are available in the region, with their errors (assumed as the standard deviation of albedo data for the families with more than one data point). With the exception of Barcelona and Tina, all families include asteroids that are likely interlopers, such as (1609) Brenda in the Gersuind family, which is a D–T asteroid in what most likely is an S-type family. Overall, the albedo data seem to confirm the possible identification of the Barcelona family as an Sq-type group, and possibly that of the Gersuind family as a S-type family, but very little else can be concluded from the available data.

Regarding the asteroid absolute magnitudes, Fig. 14(a) displays an (a, $\sin i$) projection of the asteroids with $e < 0.175$, while Fig. 14(b) shows the same for asteroids with $e > 0.175$. The location of the secular resonances is the one analytically obtained for the values of eccentricity and angles of (480) Hansa in Section 2. Small black dots display the locations of asteroids with absolute magnitude $H > 12$, medium full dots are associated with asteroids with $10 < H < 12$ and large full dots display the position of all objects with magnitude smaller than 10 for all 2310 numbered objects (no information on the absolute magnitude is available for multi-opposition asteroids).

As can be seen in the figure, the Pallas and Hansa family region is dominated by a population of small objects ($H > 12$). Overall, out of the 2310 numbered asteroids just 22 asteroids have absolute magnitude smaller than 10, and there are 20 with $10 < H < 12$ (one can safely assume that multi-opposition objects should all have $H > 12$ as well). Of the large $H < 10$ objects, only six are family members, and they are respectively (945) Barcelona, (480) Hansa, (686) Gersuind, (2) Pallas, (148) Gallia and (1222) Tina (71 Niobe, which is a member of the Gallia frequency family, is most likely an interloper). The situation is similar for medium-sized asteroids. The remaining 16 asteroids with $H < 10$ tend to concentrate in the Olympia and Atalante regions, and may be considered objects that have not been not broken up to form families (yet), which may also explain the lack of large asteroid groups in these two areas. Families in the region seem therefore to be either the result of cratering events, as seems most likely for the Pallas family, or formed by small-diameter objects, such as the Hansa and Tina families. More details on the size distribution of asteroid families will be given in the next section.

6 CUMULATIVE DISTRIBUTIONS OF FAMILY MEMBERS

The size distribution of asteroids is one of the most significant observational constraints on their history, and it is also one of the hardest quantities to determine because of strong selection effects (Parker et al. 2008). As a next step of my preliminary analysis of the Pallas and Hansa regions, I compute the cumulative H distribution $N(<H)$ (i.e. the number of objects in a group with an absolute magnitude less than a given value) for the classical and frequency families in the region. The size of a family member can be obtained using equation (6) and assuming that all members have the same albedo value, taken as the family mean value (see Table 4). Here I limit my analysis only to families in order to have statistically significant samples for the cumulative distribution. Even among families, not all groups have sufficient data. For instance, only 24 asteroids in the Pallas classical family and 21 in the Tina one have absolute magnitude data, which is not enough to provide statistically significant results. This analysis is also limited to numbered asteroids only, since multi-opposition ones do not have absolute magnitude data yet. Fig. 15 shows the cumulative H distribution $N(< H)$ for the two Hansa families, (a) classical and (b) frequency. Results are similar for the other families and will not be shown for the sake of brevity.

As is the case for several other families studied by Parker et al. (2008), family cumulative distributions for the groups in the region seem to be best approximated by a 'broken' power law, for the two intervals in H between 12 and 14 and between 14 and 15. According to Parker et al. (2008), data on absolute magnitude H were

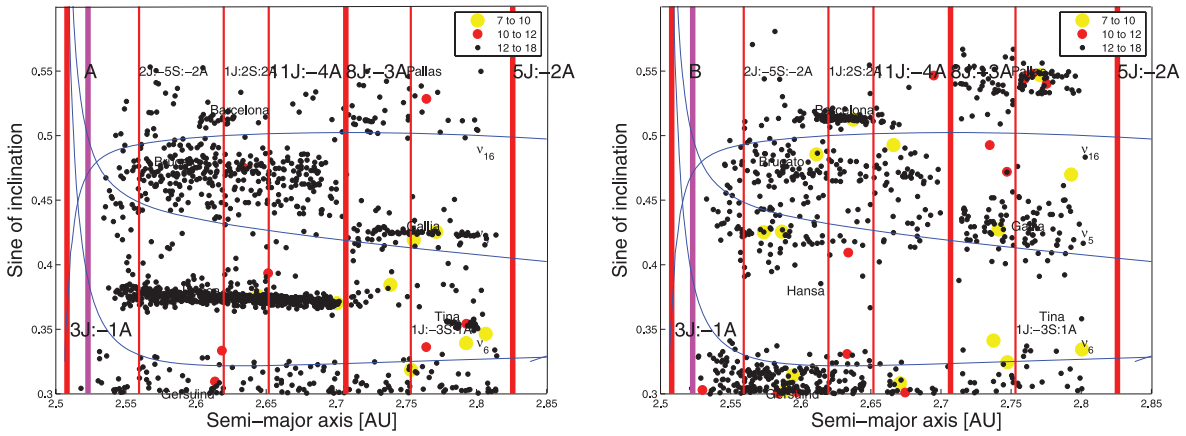

Figure 14. An (a, $\sin i$) projection of the asteroids in the region of the Pallas and Hansa families for asteroids with (a) $e < 0.175$ and (b) $e > 0.175$. Small black dots display the locations of asteroids with $H > 12$, medium full dots are associated with asteroids with $10 < H < 12$ and large full dots display the position of all objects with magnitude smaller than 10.

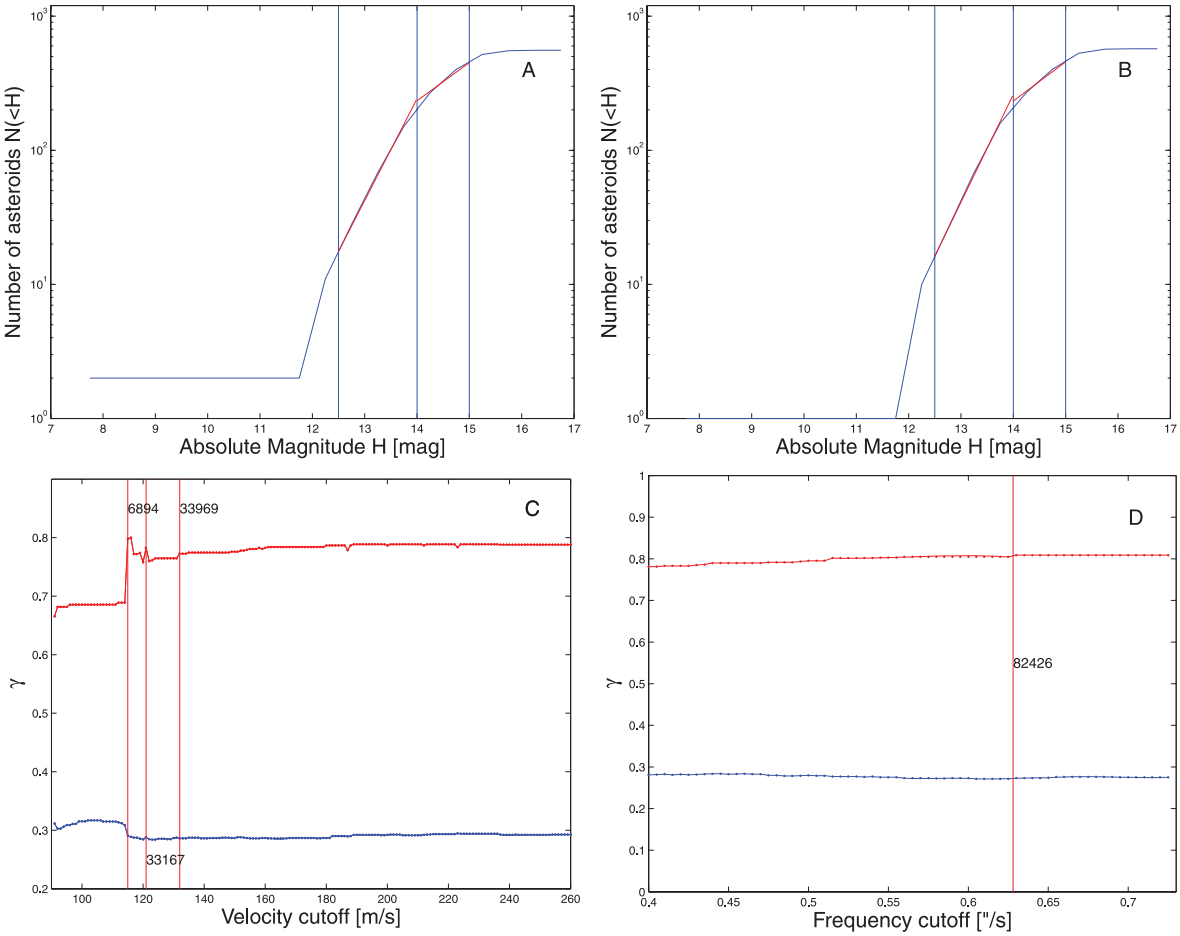

Figure 15. (a) and b display the cumulative distribution $N(>H)$ of the classical and frequency members of the Hansa family. (c) and (d) display the dependence of the exponent of the cumulative H distribution $N(<H)$ as a function of the velocity and frequency cut-offs, found in the range of absolute magnitude H (12.5, 14.0) (red lines) and (14.0, 15.0) (blue lines).

essentially complete up to magnitude 17 in the inner main belt and up to magnitude 15 in the outer one in January 2008. This, however, only applies to $\sin i < 0.3$ asteroids and absolute magnitude data may be lacking for highly inclined objects, especially at fainter magnitudes. To obtain information on the collisional evolution of the new families and to test the possible completion of highly inclined asteroid absolute-magnitude data, I computed the exponents γ_1 and γ_2 that best fit the cumulative distributions in the intervals in H between 12 and 14 and between 14 and 15, respectively.

I found that for the classical family the two exponents that best fit the two intervals are 0.760 and 0.285, respectively, while for the frequency family I obtained values of $\gamma_{1,2}$ of 0.804 and 0.274. The values of γ_1 are somewhat high (background asteroids usually have values of γ_1 of 0.61) and possibly suggest a relatively low age for the Hansa family. The values of γ_2 are instead quite low and may possibly be produced by incompleteness in the data for smaller asteroids. This situation could be improved once data on absolute magnitudes of multi-opposition asteroids become available.

In Fig. 15(c) and (d) I show the dependence of the exponent of the cumulative H distribution $N(<H)$ as a function of the velocity and frequency cut-offs[5] found in the range of absolute magnitude H (12.5, 14.0) ($\gamma > 0.5$) and (14.0, 15.0) ($\gamma < 0.5$). Vertical lines display the values of the cut-offs for which the Hansa family englobes other families and clumps in the region. As can be seen in the figure, the cumulative exponents fluctuate when the Hansa cluster englobes some of the minor groups in the region, then reaching an almost constant value for larger cut-offs. The Hansa family is limited by the powerful ν_5, ν_6 secular resonances and by the 3J:–1A and 8J:–3A mean-motion resonances, so the family merges with the local background only for very large values of the cut-off, not shown in the figure. This explains why there are no sudden drops in the γ exponents.

Values of the γ_1 and γ_2 exponents for the other families are summarized in Table 5 in the third and fourth columns (the second column reports the number of asteroids for which data on absolute magnitude are available, and the first column the name of the family (the suffix 'c' refers to classical families and suffix 'f' to frequency ones). Overall, the Barcelona, Brucato and Hansa families are characterized by relatively large values of the exponent γ_1, which could possibly suggest relatively low ages for these groups. In contrast, the Gersuind and Gallia families are characterized by lower values of γ_1, which may be compatible with a collisionally more evolved group.

In order to obtain more information on family ages I will now turn my attention to the time-scale isolines of the Yarkovsky effect.

[5] Due to its value of proper frequency g, (480) Hansa is not a member of the frequency family.

Table 5. Values of exponents of the cumulative size distributions γ_1 and γ_2 for families in the region of the Pallas and Hansa groups.

Name	$N(H)$	γ_1	γ_2
(945) Barcelona(c)	147	0.792	0.459
(945) Barcelona(f)	152	0.800	0.471
(4203) Brucato(f)	154	0.749	0.339
(480) Hansa(c)	557	0.760	0.285
(480) Hansa(f)	571	0.804	0.292
(686) Gersuind(c)	90	0.507	0.301
(686) Gersuind(f)	92	0.565	0.347
(148) Gallia(c)	49	0.637	0.371
(148) Gallia(f)	62	0.579	0.416

7 YARKOVSKY ISOLINES AND *C*-TARGET FUNCTIONS

Now that I have revised the information in the literature on geometric albedos and absolute magnitude, I am equipped to start setting constraints on an age estimate for families in the region. In Vokrouhlický et al. (2006), the authors used the (a, H) distribution of asteroid families to determine their ages. In particular, the authors introduced a target function C, defined as

$$0.2H = \log_{10}(\Delta a/C), \tag{7}$$

where $\Delta a = a - a_c$ and a_c is the 'central' value of semi-major axis of the family members. The most appropriate definition of the family centre relates to the concept of a barycentre. I took

$$a_c = \sum_{i=1}^{n_{ast}} \frac{a M_i}{M_{tot}}, \tag{8}$$

where n_{ast} is the number of family members and M_i is the mass of each asteroid, estimated assuming that all asteroids can be approximated as spheres using a density of 2500 kg m^{-3} for asteroids in the S complex and 1500 kg m^{-3} for asteroids in the C complex and a diameter obtained via equation (6). For asteroids for which the geometric albedo is not available, I used the mean value of the albedo reported in Table 4. Equations similar to equation (8) hold for e_c and i_c. With these approximations, I found that the total mass M_{tot} of the Barcelona families is of the order of 1.47×10^{17} kg, that its barycentre is at $a_c = 2.636$ au and that $\simeq$78 per cent of the current family mass is inside the largest body. Data for the other families are reported in Table 6. The mass of (2) Pallas [$(1.17 \pm 0.03) \times 10^{-10}$ M$_\odot$] is taken from Goffin (2001). In computing the family barycentres, I have excluded from the computation of the total mass obvious interlopers such as (925) Alphonsine (an S-type asteroid of low absolute magnitude $H = 7.78$ very far from the family barycentre) for the Hansa family and (71) Niobe (a X-type object in what appears to be an S-type family) for the Gallia frequency family.

Now that the values of family barycentres are computed, it is possible to obtain estimates on the upper limits of family ages by computing the time needed for an asteroid of a given size to cover the distance from the family centre to the extreme values in a of the family. Fig. 16(a) shows an (a, H) projection of Hansa classical-family members. This figure also shows the distance covered by asteroids to diffuse from the centre of the family via the Yarkovsky effect, computed using the Vokrouhlický (1999) model of the diurnal version of the Yarkovsky effect, for spherical bodies and in the linear approximation for heat conduction in a spherical, solid and rotating body illuminated by solar radiation. I used the following parameters to describe the Yarkovsky force: thermal conductivity $K = 0.0001$ W m^{-1} K^{-1}, specific heat capacity $C_p =$ 680 J kg^{-1} K^{-1}, density 2500 kg m^{-3} for S-complex asteroids and 1500 kg m^{-3}, surface density 1500 kg m^{-3}, bond albedo 0.11 and the mean geometric albedo appropriate for each family (Section 5). With these parameters, using the barycentric value of the family a-distribution a_c and assuming a rotation period inversely proportional to the radius (Farinella, Vokrouhlický & Hartmann 1998), I obtained lines of maximal Yarkovsky drift for the Hansa classical family for an age of 1600 Myr. Since I am not considering the effect of the primordial-ejection velocity field, this sets upper limits on the possible age of the family.

Fig. 16(b) shows the values of the C target function for the Hansa classical family.[6] As can be seen in the figure, the C distribution has two peaks and is not symmetrical. The excess of positive C values may possibly be associated with an excess of original prograde rotators, as observed in the Padua family among others (Carruba 2009). Further study is however needed to confirm this hypothesis.

Data on family upper-limit age estimates for the other families are available in the fifth column of Table 6. The Barcelona family seems to be a relatively young group, with an age of at most 350 Myr, which seems to confirm the results from the cumulative size exponents. It has an asymmetrical distribution in semi-major axis, with most of its members having values of a smaller than that of the family barycentre. This depletion may be possibly caused by the presence of the 11J:–4A mean-motion resonance in the area.

The Brucato family (if indeed is a real collisional family, which seems not to be confirmed by the taxonomical analysis) appears to have a greater age of at most 1300 Myr and a symmetrical distribution in the (a, H) plane. The Gersuind family also has a symmetrical distribution in the (a, H) plane and seems to be a relatively evolved family with 800 Myr as an upper limit on its age.

Regarding the Pallas families, there are very few members in the classical (35) and frequency (79) group, so any information on Yarkovsky isolines may suffer from the paucity of data. Both families have an upper-limit estimate of the age of 500 Myr, while an upper limit of 450 Myr applies for the Gallia families. Finally the Tina family seems to be a very young group, with an age of 150 Myr at most.

8 LIGHT CURVES AND ROTATION-RATE ANALYSIS

It has been recently proposed that binary asteroids can be formed because of the increase in the rotation rate of the parent body caused by the Yarkovsky–O'Keefe–Radzievskii–Paddack (YORP) effect (Pravec et al. 2008). Obtaining information on asteroid periods is therefore of significant importance in understanding their dynamical evolution. Here I have revised the current information available for members of families in the region in the Asteroid Light-Curve Data base (LCDB: Warner et al. 2008) as of March 2010. Of the 4310 asteroids in the Pallas and Hansa family regions, 39 have a period estimate in the LCDB.

Fig. 17 displays a histogram of the distribution of rotation frequencies for the 39 asteroids for which such information is available. Of these objects, 15 are family members (two belong to the Barcelona family, three to the Hansa one, four to the Gersuind group, four to the Pallas family and two to the Gallia group). The sample is too limited to allow statistically significant information to

[6] I computed the observed data $N_{obs}(C)$ for the classical and frequency families, obtained by $(C, C + \Delta C)$ binning with $\Delta C = 5 \times 10^{-7}$.

Table 6. Barycentre, total mass and upper limits for families in the region.

Name	a_c (au)	M_{tot} (10^{17} kg)	M_L/M_{tot} (per cent)	Est. age (Myr)
(945) Barcelona(c)	2.636	1.48	77.2	350
(945) Barcelona(f)	2.636	1.46	78.4	350
(4203) Brucato(f)	2.628	2.02	7.8	1300
(480) Hansa(c)	2.644	38.7	90.6	1600
(480) Hansa(f)	2.641	36.8	95.1	1600
(686) Gersuind(c)	2.585	4.80	62.5	800
(686) Gersuind(f)	2.587	4.57	65.5	800
(2) Pallas(c)	2.771	2267.7	99.9	500
(2) Pallas(f)	2.771	2267.7	99.9	500
(148) Gallia(c)	2.771	26.6	99.7	450
(148) Gallia(f)	2.771	26.6	99.7	450
(1222) Tina(c)	2.792	0.2	82.1	150
(1222) Tina(f)	2.792	0.2	79.9	150

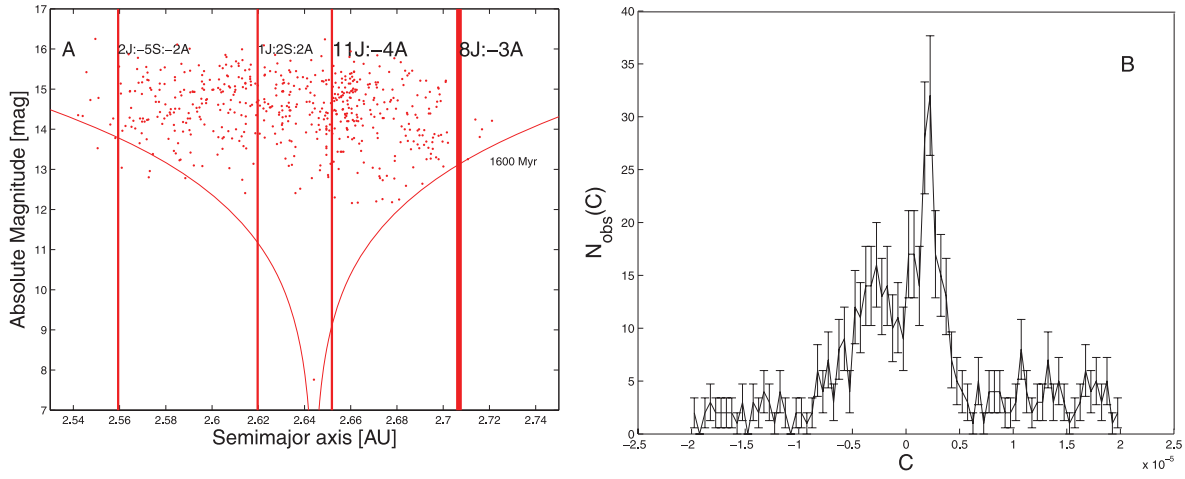

Figure 16. (a) An (a, H) projection of the members of the classical Hansa family. (b) Values of the C target function for the same family.

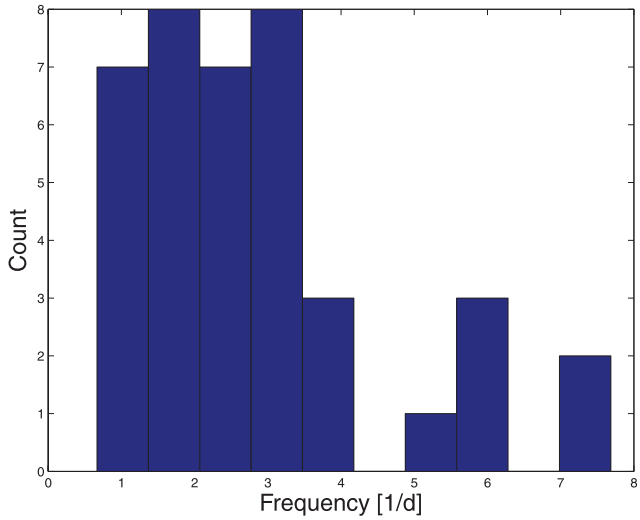

Figure 17. Histograms of rotation frequencies (in d^{-1}) for the 39 asteroids present in the Asteroid Light Curve Data Base.

be obtained, but it can be noted that there are 19 objects with periods longer than a day. As found by Warner et al. (2009) for asteroids in the Hungaria region, there seems to be an excess of slow rotators. This could possibly be caused by the YORP effect, with the excess of slow rotators related to the longer time slowly rotating objects spend in that state (Pravec et al. 2008).

9 DYNAMICS IN THE REGION OF THE PALLAS AND HANSA FAMILIES

A preliminary discussion on the dynamics in the region of the Pallas and Hansa families was carried out in Section 2.1. To gain further insights on the distribution of mean-motion and secular resonances in the region, I integrated 7000 particles in (a, e) space, 7000 particles in (a, $\sin i$) space and 10 000 particles in (e, $\sin i$) space. I used a step of 0.005 au in a, 0.005 in e and 0.°2 in i, and took particles in an equally spaced grid of 70 by 100 particles in the (a, e) plane, 70 by 100 particles in the (a, $\sin i$) plane and 100 by 100 particles in the (e, $\sin i$) plane.[7] The initial values of $\sin i$, e, a (for the simulations in the (a, e), (a, $\sin i$) and (e, $\sin i$) planes, respectively) and initial angular elements Ω, ω and λ of the test particles were fixed at those of (40971) 1999 TY264, a high-e asteroid in the Hansa family that was already used in Carruba & Michtchenko (2009) to obtain families in the domains of proper elements and colours and proper frequencies and colours. I choose this asteroid to avoid the problem of proper frequency determination associated

[7] My particles covered a range between 2.5 and 2.85 au in a, 0 and 0.5 in e and 15° and 35° in i, respectively.

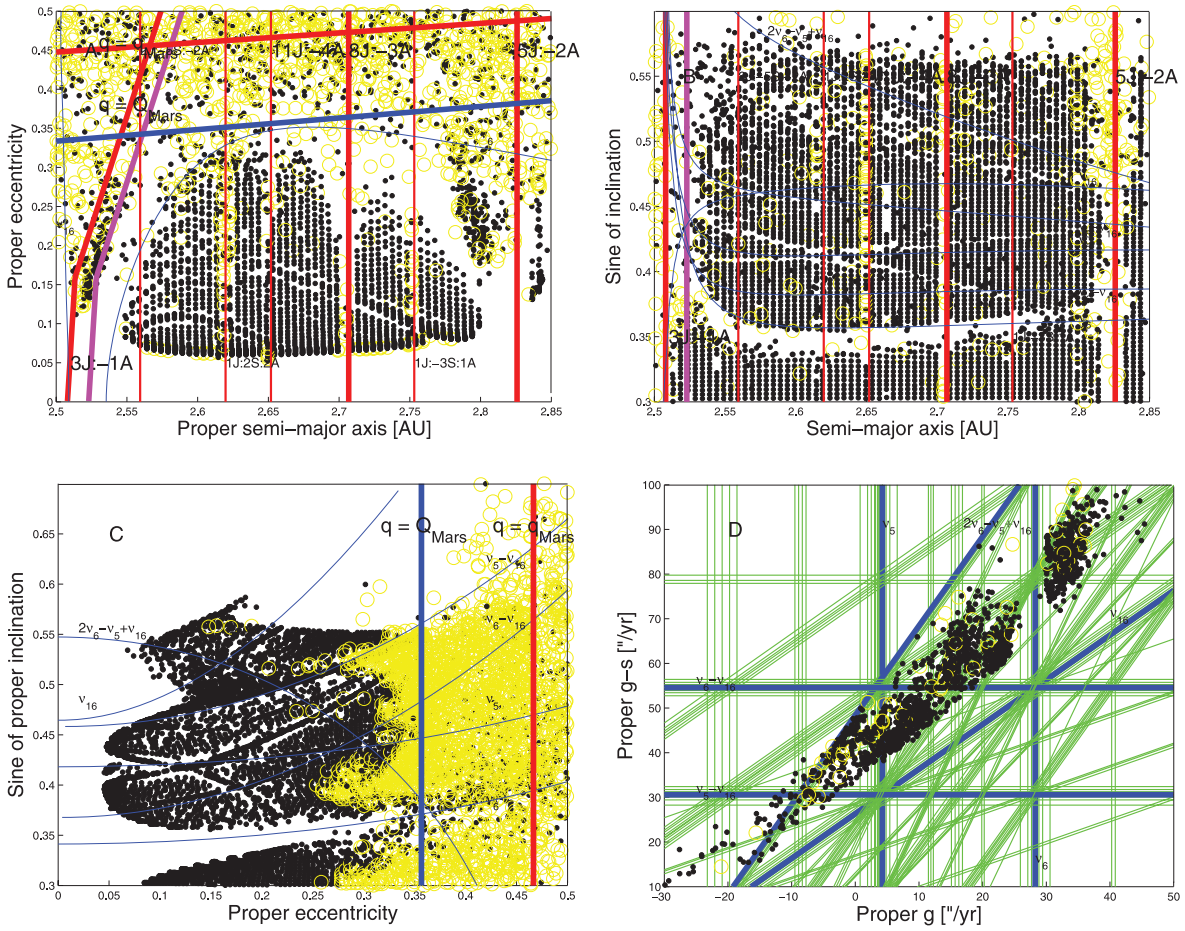

Figure 18. (a) (a, e), (b) $(a, \sin i)$ and (c) $(e, \sin i)$ projections of averaged elements for test particles in the region of the Pallas and Hansa families. (d) displays a $(g, g + s)$ projection of asteroid proper frequencies, with the location of the main secular resonances in the region.

with the low-eccentricity objects in the Hansa family, such as (480) Hansa itself.

Fig. 18 displays (a) (a, e), (b) $(a, \sin i)$ and (c) $(e, \sin i)$ projections of averaged elements for test particles in the region of the Pallas and Hansa families. Averaged elements are not constant in motion over millions of years as proper elements, but provide a qualitative insight on the local dynamics. Circles display Lyapunov times $T_{\rm L}$ smaller than 20 000 yr, while black dots are associated with times larger than 20 000 yr. The maximum Lyapunov exponent (MLE: Lyapunov 1907) is a measure of exponential stretching of nearby orbits. The Lyapunov exponents are equal to zero for regular orbits (they tend to zero in finite-time calculations), while they assume positive values for chaotic orbits. The inverse of a Lyapunov exponent is the Lyapunov time $T_{\rm L}$. Smaller values of $T_{\rm L}$ indicate enhanced local stochasticity. Lyapunov times were computed with the same procedures discussed in Carruba (2009).

Vertical lines display the location of mean-motion resonances, as discussed in Section 2, while blue lines show the location of the centres of the secular resonances that appeared in the map.[8]

As can be seen in Fig. 18(a), it is easy to spot the chaotic region with $q = Q_{\rm Mars}$ characterized by close encounters with Mars. This region is also clearly noticeable in the $(e, \sin i)$ plane (Fig. 18c). At lower eccentricities the presence of the ν_6 secular resonance destabilizes several of the test particles by increasing their eccentricity to Mars-crossing levels with a mechanism described in Carruba (2010). Other chaotic regions are associated with the separatrixes of mean-motion resonances such as the 3J:–1A, 5J:–2A, 8J:–3A and 1J:2S:2A.

The inclined alignment in the dynamical maps at $\simeq a$ =2.75 au and $e \simeq 0.1$ is caused by non-linear secular resonances such as $\nu_{16} + \nu_5 - \nu_6$. Since no real asteroid was found inside this resonance, I did not plot the resonance centre in this picture. Later on, the effect of other secular resonances will be discussed in more detail.

Finally, the fact that averaged eccentricities did not reach zero values arises from the fact that for asteroids in the Hansa region the forced eccentricity is larger than the free one, so that asteroids with small proper eccentricity are projected to their values of the forced one in the space of averaged elements.

More interesting and physically significant are the results shown in the space of $(a, \sin i)$ (Fig. 18b). The effect of the linear secular resonances ν_5, ν_6 and ν_{16} is clearly visible in this map. Three non-linear secular resonances have a significant population of objects to within the $\pm$ 0.3 arcsec yr^{-1} limit that Carruba (2009) show to be the location where 95 per cent of resonant objects are found: the $\nu_6 - \nu_{16}$, $\nu_5 - \nu_{16}$ and $2\nu_6 - \nu_5 + \nu_{16}$ secular resonances. These resonances are shown as blue lines in Fig. 18(b) and interact with members of the dynamical groups found in this work. More

[8] The location of secular resonances in the space of averaged proper elements is different from that in the space of proper elements.

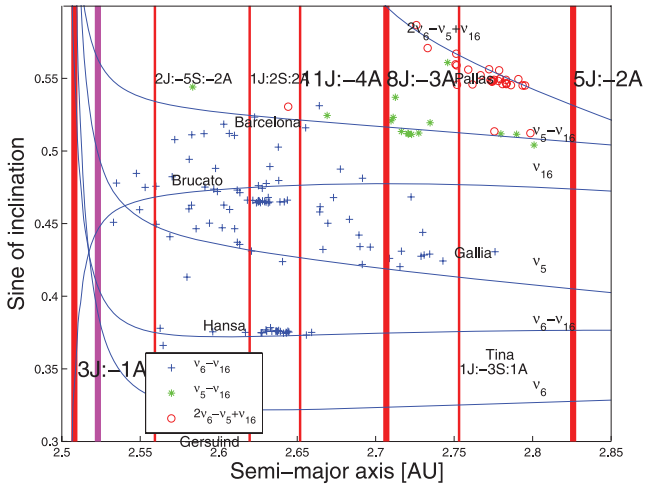

Figure 19. Orbital location in the (a, $\sin i$) plane of the asteroids in the $\nu_6 - \nu_{16}$ (blue crosses), $\nu_5 - \nu_{16}$ (green asterisks) and $2\nu_6 - \nu_5 + \nu_{16}$ (red circles) resonances.

information on this will be provided later on in this section. Two other secular resonances, the $2\nu_5 + \nu_{16}$ and the $\nu_5 + \nu_6 + \nu_{16}$, are responsible for some of the inclined alignments in the dynamical map but have just one asteroid to within the ± 0.3 arcsec yr^{-1} boundary (2000 YZ14 and 2004 DT39, respectively) and are therefore not shown in the figure.

Another very interesting feature is the limited amount of chaotic behaviour associated with the boundaries of the ν_5, ν_6 and ν_{16} secular resonances when compared with analogous results in the region of the Phocaea family (Carruba 2009, 2010). As discussed in Carruba (2010), the chaotic behaviour near the ν_6 secular resonance was caused by the fact that the resonance pushed asteroid eccentricities to a region of shallow Mars-crossing orbits ($e > 0.31$) when the difference in $|g - g_6|$ was less than 2.55 arcsec yr^{-1}. In this region asteroids had still pericentres lower than the aphelion of Mars, but were exposed to a series of shallow Martian close encounters that destabilized them over time-scales of 200 Myr or less. Eccentricities for reaching Mars-crossing orbits are, however, larger in the Pallas and Hansa region and it is possible that the semi-stable area at $e > 0.31$ found in the Phocaea region could be significantly smaller in the Pallas and Hansa region. This could explain why the chaotic layer near the ν_6 secular resonance is more limited in this area. Further study is, however, needed to test this hypothesis quantitatively.

Fig. 18(c) shows an (e, $\sin i$) projection of averaged elements of particles in the area. One may notice a chaotic region with eccentricity lower than that needed to reach the Martian apocentre, which is a region associated with shallow close encounters with Mars. The long-term stability of this region is an interesting topic for future research.

Finally, Fig. 18(d) displays the orbital location in the (g, $g - s$) plane of the numbered asteroids for which information on the Lyapunov time is available at the AstDyS site. Thin lines show the location of all secular resonances up to order 6, while thick lines are associated with resonances that have a resonant population larger than 1. One may clearly notice the alignment of asteroids in the $\nu_6 - \nu_{16}$, $\nu_5 - \nu_{16}$ and $2\nu_6 - \nu_5 + \nu_{16}$ secular resonances.

Fig. 19 displays the orbital location in the (a, $\sin i$) plane of the asteroids in the $\nu_6 - \nu_{16}$ (crosses, 105 objects), $\nu_5 - \nu_{16}$ (asterisks, 15 objects) and $2\nu_6 - \nu_5 + \nu_{16}$ (circles, 29 objects) resonances, to within 0.3 arcsec yr^{-1}. The $\nu_6 - \nu_{16}$ secular resonance interacts with the Hansa, Brucato, Barcelona and Gallia families. Understanding the long-term effect of this interaction, also using a distance metric in the (n, g, $g - s$) domain as in Carruba & Michtchenko (2009), may be an interesting challenge for future works. This may be particularly important for the Brucato family, which is observable only as a clump in proper-element space and may be significantly affected by secular dynamics.

The other two resonances, and in particular the $2\nu_6 - \nu_5 + \nu_{16}$ (a $g + s$ non-linear resonance), interact mostly with the Pallas family. It is worth noticing that Pallas is in a near 1:1 mean-motion orbital resonance with Ceres (Goffin 2001). Pallas also has a near 18:7 resonance (6500-yr period) and an approximate 5:2 resonance (83-yr period) with Jupiter (Taylor 1982). Further exploration of the dynamics of Pallas and its families is a very interesting subject for possible future research.

10 CONCLUSIONS

In this work I have investigated the current status of the knowledge of asteroids in the region of the Pallas dynamical family. Among other things I have done the following.

(i) Obtained values of synthetic proper elements for 2310 numbered and 2142 multi-opposition objects. With respect to published AstDyS values, 26 numbered objects had discrepancies in the values of proper e and 368 objects had discrepancies in the proper g values, which are connected mostly with the problem of obtaining values of g for objects with $e_{\rm free} < e_{\rm forced}$. These discrepancies are essentially intrinsic to the method used by Knežević & Milani (2000) to obtain synthetic proper elements. The larger sample of proper elements obtained by also considering multi-opposition objects was quite useful for asteroid family determination.

(ii) Identified asteroid families and clumps in this region using CHCM and FHCM. My analysis shows that the Gallia and Barcelona clumps of Gil-Hutton (2006) should now be considered proper dynamical families, in both proper-element and frequency domains. A new family around (1222) Tina was identified for the first time in this work in both proper-element and frequency domains. A frequency family around (4203) Brucato (the group appears as a clump in the proper-element domain) was also found, as well as nine other clumps, one of which (36240 1999 VN44) appears in both domains and is a good candidate for being the result of a real collisional event. Family subgroups and asteroid-pair candidates (Pravec & Vokrouhlický 2009; Milani et al. 2010) were also identified in the region.

(iii) Revised the current state of knowledge on the taxonomy of objects in the Pallas and Hansa family regions and found that the Hansa family could be taxonomically compatible with an S-type group, while the Pallas one is mainly composed of B-type objects (with two C-type asteroids as members as well). No sufficient information is available on the other groups found in this work to allow any other conclusions to be drawn.

(iv) Obtained principal components based on SDSS-MOC3 data, and used this information to obtain families in the space of colours and proper elements and colours and proper frequencies (Carruba & Michtchenko 2007; Carruba 2000). The Barcelona family seems to be consistent with an Sq-type composition, the Pallas family is compatible with a B-type composition and the Gersuind, Gallia and Tina families should belong to the S complex. Due to the presence of asteroids belonging to both the C- and X-type complexes, the

Brucato frequency family may not be the product of a collisional event.

(v) Revised the current knowledge of absolute magnitudes and geometric albedos for objects in the region. The albedo data seem to confirm that the Barcelona and (possibly) Gersuind families could belong to the S-type complex. The region is dominated by smaller bodies ($H > 12$), with the presence of very few (22) large ($H < 10$) asteroids (2 Pallas being one of the most notable exceptions). The 16 large asteroids that do not belong to the families tend to concentrate in the Olympia and Atalante regions, which are characterized by the lack of large asteroid groups.

(vi) Computed the cumulative absolute magnitude H distribution ($N(< H)$) for families in this region. As in Parker et al. (2008), the family distribution seems to be best approximated by a broken power law for two intervals in H between 12 and 14 and between 14 and 15. The exponents of the cumulative size distribution seem to suggest a relatively low age for the Barcelona and Brucato families, and higher ages for the Gersuind and Gallia ones.

(vii) Obtained Yarkovsky isolines and C-target function values (equation 7) for members of families in this region. I obtained an upper limit for the family ages of 350 Myr for the Barcelona families, 1300 Myr for the Brucato frequency family, 1600 Myr for the Hansa groups, 800 Myr for the Gersuind clusters, 500 Myr for the Pallas ones, 450 Myr for the Gallia families and 150 Myr for the Tina ones. Asymmetries in the semi-major axis distribution of family members, possibly caused by an excess of original prograde rotators or by local dynamics, are observed in the Barcelona and Hansa families.

(viii) Studied the available information on rotation rates for asteroids in the Pallas and Hansa family regions (Warner, Harris & Pravec 2008). 39 bodies have estimates for their rotation periods, and a histogram of the rotation frequencies shows that there is an excess of slow rotators, explainable in the framework of the evolution of the spin axis via the YORP effect.

(ix) Obtained dynamical maps of averaged elements for grids in (a, e), (a, $\sin i$) and (e, $\sin i$) of osculating initial conditions and identified the mean-motion and secular resonances that seem to have the largest effect on the short-term (20 Myr) stability of the asteroid averaged elements. The chaotic layer near the ν_6 secular resonance is of more limited dimensions than the one found in the Phocaea family region. Also, I found that the Brucato and Hansa families are characterized by their interaction with the $\nu_6 - \nu_{16}$ secular resonance, while the Pallas one is crossed by the $2\nu_6 - \nu_5 + \nu_{16}$ secular resonance. Several quasi-resonances with Jupiter and Ceres are present in the region of the Pallas families.

Among the issues not covered in this paper, the search for very close pairs of asteroids (Pravec & Vokrouhlický 2009) using the successive filtering approach of Milani et al. (2010) could be a very appealing topic of research, as well as the search for family subgroups. The candidates obtained in this work (see Table 1) passed just the first of the filters applied by Milani et al. (2010) and need further confirmation. I believe that this topic exceeds the purpose of this work, which was first and foremost to obtain synthetic proper elements for the region of the Hansa and Pallas families, obtain dynamical and spectroscopic families and review the current status of our knowledge regarding asteroids in the region. However, it remains an interesting topic of research for future work.

Another interesting line of research, in my opinion, could be studying the limited extent of chaotic dynamics near the boundaries of the ν_6, ν_5 and ν_{16} secular resonances, when compared with results around the ν_6 resonance in the Phocaea family region (Carruba 2009, 2010). The possibility that a region of semi-stable orbits at high eccentricities that experience shallow Martian close encounters could be of more limited extension in the region of the Pallas and Hansa families, because of the larger values of eccentricity needed to reach Mars-crossing orbits in the area and, possibly, of the resonance topologies, is in my opinion interesting and worth exploring in a future paper.

The long-term stability of some of the groups found in this work is also a very appealing possible topic of research. Exploring the statistical significance of the clumps identified in the space of proper elements and frequencies when the Yarkovsky effect is considered is important, especially considering the limited amount of information available on the taxonomy for some of these groups.

The effect of non-linear secular resonances, such as the $\nu_6 - \nu_{16}$ one, on the Hansa and Brucato families may possibly explain some of the discrepancies found in this work, such as the fact that the Brucato family is just a clump in the proper-element domain. The use of the (n, g, $g - s$) distance metric may provide useful information for such families.

A very different region seems to be the one associated with the Pallas families, which is characterized by the presence of the $2\nu_6 - \nu_5 + \nu_{16}$ secular resonance and by several quasi-resonances with Jupiter and Ceres. Understanding the complex dynamics of the region is a challenge for future papers.

More important than the effect of non-linear resonances is, however, the effect of linear resonances such as the ν_6. It has long been known that (1222) Tina was in an apocentric librating state of the ν_6 (Morbidelli & Henrard 1991). In such a state the resonant argument σ of the ν_6 resonance, $\varpi - \varpi_6$, oscillates around the stable point at 180°, rather than around 0° as is the case for librating orbits. Preliminary results (Carruba & Winter 2010) suggest that all members of the Tina families (classical and frequency) are currently in such a state, making the Tina family the first group in the Solar system to be completely inside a secular resonant configuration. The very interesting dynamics of the Tina family will be further investigated in future works.

Finally, the use of a Monte Carlo model that includes Yarkovsky and YORP effects, as has been done for the Padua family (Carruba 2009) and other cases, could help in obtaining better estimates for the ages of the younger groups found in this work.

As often in science, this work has answered some questions but produced several new ones, in many cases completely unanticipated when this work started. The large number of unanswered questions is once again proof of the vitality of asteroid dynamics as a field of research.

ACKNOWLEDGMENTS

I am grateful to an unknown reviewer for revision of my paper. I thank the São Paulo State Science Foundation (FAPESP), which supported this work via grant 06/50005-5, and the Brazilian National Research Council (CNPq, grants 302183/2008-6 and 473345/2009-9). I am also grateful to Dr Tatiana A. Michtchenko for several discussions on the peculiar nature of the proper frequencies of Hansa family members and to Professor Dr Kleomenis Tsiganis for a helpful conversation on asteroid synthetic proper elements. I thank Professor Dr Silvia G. Winter for reading and correcting the last version of this paper. Finally, I am also grateful to the department of Mathematics of FEG-UNESP for the use of their facilities.

REFERENCES

Beaugé C., Roig F., 2001, Icarus, 153, 391
Bendjoya P., Zappalà V., 2002. Asteroids III. Univ. Arizona Press, Tucson, p. 613
Brož M., 1999, Thesis, Charles Univ., Prague
Brož M., Vokrouhlický D., 2008, MNRAS, 390, 715
Bus J. S., Binzel R. P., 2002a, Icarus, 158, 106
Bus J. S., Binzel R. P., 2002b, Icarus, 158, 146
Carruba V., 2009, MNRAS, 398, 1512
Carruba V., 2010, MNRAS, 403, 1834
Carruba V., Michtchenko T., 2007, A&A, 475, 1145
Carruba V., Michtchenko T., 2009, A&A, 493, 267
Carruba V., Winter O. C. 2010, Nat. Commun., submitted
Farinella P., Vokrouhlický D., Hartmann W. K., 1998, Icarus, 132, 378
Fukugita M., Ichikawa T., Gunn J. E., Doi M., Shimasaku K., Schneider D. P., 1996, AJ, 111, 1748
Gil-Hutton R., 2006, Icarus, 183, 93
Goffin E., 2001, A&A, 365, 627
Guillens S. A., Vieira Martins R., Gomes R. S., 2002, AJ, 124, 2322
Hergenrother C. W., Larson S. M., Spahr T. B., 1996, Bull. Am. Astron. Soc., 28, 1097
Knežević Z., Milani A., 2000, Cel. Mech. Dyn. Astron., 78, 17
Knežević Z., Milani A., 2003, A&A, 403, 1165
Lazzaro D., Angeli C. A., Carvano J. M., Mothé-Diniz T., Duffard R., Florczak M., 2004, Icarus, 172, 179
Lemâitre A., Morbidelli A., 1994, Cel. Mech., 60, 29
Levison H. F., Duncan M. J., 1994, Icarus, 108, 18
Lyapunov A. M., 1907, Ann. Fac. Sci. Univ. Toulouse, 9, 203
Milani A., Knežević Z., 1994, Icarus, 107, 219
Milani A., Knežević Z., Novaković B., Cellino A., 2010, Icarus, 207, 769
Michtchenko T. A., Lazzaro D., Carvano J. M., Ferraz-Mello S., 2010, MNRAS, 401, 2499
Morbidelli A., Henrard J., 1991, Cel. Mech. Dyn. Astron., 51, 169
Morbidelli A., Vokrouhlický D., 2003, Icarus, 163, 120
Murray C. D., Dermott S. F., eds, 1999, Solar System Dynamics. Cambridge Univ. Press, Cambridge
Nesvorný D., Jedicke R., Whiteley R. J., Ivezić Ž., 2005, Icarus, 173, 132
Parker A., Ivezić Ž., Jurić M., Lupton R., Sekora M. D., Kowalski A., 2008, Icarus, 198, 138
Pravec P., Vokrouhlický D., 2009, Icarus, 204, 580
Pravec P. et al., 2008, Icarus, 197, 497
Roig F., Gil-Hutton R., 2006, Icarus, 183, 411
Šidlichovský M., Nesvorný D., 1997, Cel. Mech. Dyn. Astron., 65 137
Taylor D. B., 1982, MNRAS, 199, 255
Tedesco E. F., Noah P. V., Noah M., Price S. D., 2002, AJ, 123, 1056
Tholen D. J., 1989, in Binzel R. P., Gehrels T., Matthews M. S., eds, Asteroid Taxonomic Classifications. University of Arizona Press, Tucson, p. 298
Vokrouhlický D., 1999, A&A, 344, 362
Vokrouhlický D., Brož M., Bottke W. F., Nesvorný D., Morbidelli A., 2006, Icarus, 182, 118
Warner B. D., Harris A. W., Pravec P., 2008, Asteroid Light Curve Data Base (LCDB) (http://www.MinorPlanetObserver.com)
Warner B. D., Harris A. W., Vokrouhlický D., Nesvorný D., Bottke W. F., 2009, Icarus, 398, 1512
Williams J. G., 1992, Icarus, 96, 251
Xu S., Binzel R. P., Burbine T. H., Bus S. J., 1995, Icarus, 115, 1
Zappalà V., Cellino A., Farinella P., Knežević Z., 1990, AJ, 100, 2030
Zappalà V., Bendjoya P., Cellino A., Farinella P., Froeschlé C., 1995, Icarus, 116, 291
Zellner B., Tholen D. J., Tedesco E. F., 1985, Icarus, 61, 355

This paper has been typeset from a TEX/LATEX file prepared by the author.